Progress In Electromagnetics Research, Vol. 143, 773–819, 2013

SILICON MULTIMODE PHOTONIC INTEGRATED DEVICES FOR ON-CHIP MODE-DIVISION-MULTIPLEXED OPTICAL INTERCONNECTS

Daoxin Dai[1], Jian Wang[1], and Sailing He[1, 2, *]

[1]State Key Laboratory for Modern Optical Instrumentation, Centre for Optical and Electromagnetic Research, Zijingang Campus, Zhejiang University, Hangzhou 310058, China

[2]JORCEP, Department of Electromagnetic Engineering, Royal Institute of Technology, S-100 44 Stockholm, Sweden

(*Invited Review*)

Abstract—Multimode spatial-division multiplexing (SDM) technology has attracted much attention for its potential to enhance the capacity of an optical-interconnect link with a single wavelength carrier. For a mode-multiplexed optical-interconnect link, the functional elements are quite different from the conventional ones as multiple modes are involved. In this paper we give a review and discussion on multimode photonic integrated devices for mode-multiplexed optical-interconnects. Light propagation and mode conversion in tapered waveguides as well as bent waveguides are discussed first. Recent progress on mode converter-(de)multiplexers is then reviewed. The demands of some functional devices used for mode-multiplexed optical-interconnects are also discussed. In particular, the fabrication tolerance is analyzed in detail for our hybrid demultiplexer, which enables mode-/polarization-division-(de)multiplexing simultaneously.

1. INTRODUCTION

As modern microprocessors include tens to hundreds of cores on a single die for adequate performance, a very large bandwidth ($\sim 10^2$ Tbit/s) is needed for the data communication between the cores and the local/distant caches as well as the off-chip main memory [1, 2].

Received 10 November 2013, Accepted 5 January 2014, Scheduled 27 January 2014

* Corresponding author: Sailing He (sailing@jorcep.org).

The capacity of an interconnect link must be further improved because the number of cores will continue to increase to > 1000 in the following years as many industry pundits predict [3]. To meet the bandwidth challenge for data communication, optical interconnects are regarded as a very promising solution [1, 2], because one can utilize advanced photonic multiplexing technologies [3], including wavelength-division-multiplexing (WDM), polarization-division multiplexing (PDM), and spatial-division multiplexing (SDM), which have been developed and used for long-haul optical fiber communications.

For example, a 4-channel coarse WDM (CWDM) link with 400 GHz channel-spacing has been used to realize a 50 Gbps communication link between two chips [4]. However, it will be very expensive to realize a dense WDM (DWDM) optical interconnect link with several tens or even hundreds of channels considering the complicated, expensive, and power-consuming management for wavelength tuning, conversion, routing and switching in DWDM systems. Therefore, it is interesting and necessary to enhance the link capacity with low-cost single-wavelength carrier light. In this case, the PDM and SDM technologies become very useful.

It is noted that the polarization state of light can be maintained very well for the case of on-chip optical interconnects. Therefore, on-chip PMD technology can be realized conveniently to double the link capacity by using polarization handling devices including polarization beam splitters (PBSs) and polarization rotators. In recent years, people have developed various polarization handling devices based on different structures/materials (see e.g., our recent review on this [5]). In this paper we focus on the SDM technology, which has attracted intensive attention for long-haul optical fiber communications to improve the capacity by using multi-core [6] as well as multimode optical fibers or waveguides [7, 8]. The SDM technology is also attractive for optical interconnects in data centers where upgrading an existing network or installing a new network is relatively simple [9–12]. It becomes even more convenient to apply the SDM technology to photonic networks-on-chip because planar optical waveguides can be fabricated precisely within the chip to control accurately the propagation of guided-modes and the eigen-modes could be converted, transferred or coupled conveniently between planar optical waveguides with some specific structures.

In comparison with the multi-core SDM technology, the multimode SDM technology [13–15] provides a means of achieving more concise photonic integrated circuits (PICs) as only one multimode bus waveguide is included and each eigen-mode in the multimode bus waveguide carries different data. One can easily combine the multi-core

SDM and the multi-mode SDM when necessary. One should note that the drawback for the multi-core SDM technology is the large footprint and the increased layout complexity especially when too many channels are included. In addition, a significant excess loss might be introduced due to the waveguide crossings, which are usually indispensable for large-scale PICs. Therefore, in this paper we focus on the multimode SDM technology.

For the multimode SDM, which has been proposed to enhance the capacity of fiber optical communications [7, 8], the difficulty is to realize mode (de)multiplexers for handling higher-order modes in a multimode optical fiber/waveguide. In order to reduce the complexity, few-mode fibers have been developed and the few-mode (de)multiplexing is realized with some complicated free-space optical setups [16–25], which, however, is very difficult to extend to include additional modes. For photonic networks-on-chip, the situation becomes much better because multi-mode planar optical waveguides can be precisely fabricated to manage the propagation of multi-modes and some specific PICs can be designed to realize the conversion between the eigen-modes conveniently [14]. However, for a multimode SDM optical-interconnect link, the higher-order mode handling has to be very meticulous to avoid any undesired mode coupling/conversion so that the channel crosstalk can be low. For example, the bending radius of a multimode waveguide has to be large to minimize the mode-coupling crosstalk [26]. In this paper, we first give a discussion on the configuration and the device demands for a multimode SDM optical-interconnect link. Light propagation along bent and tapered multimode waveguides is also discussed. Silicon mode (de)multiplexing technologies and devices reported recently are then reviewed, particularly some mode converter-multiplexers as one of the most important key components.

2. THE CONFIGURATION FOR A MULTIMODE SDM OPTICAL-INTERCONNECT LINK AND THE DEVICE DEMANDS

For any optical interconnect link with N channels multiplexed, one must have a transmitter to generate the N-channel data and a receiver to receive the N-channel data. For a mulitmode SDM system discussed here, all the channels have the same wavelength while each eigen-mode in a multimode bus waveguide carries different data. Therefore, only one laser diode (LD) with a fixed wavelength is needed for all the N channels, which can lower the cost greatly. In order to realize a multimode SDM optical-interconnect link with N-channels, we can take several approaches as shown in Figs. 1(a)–(c).

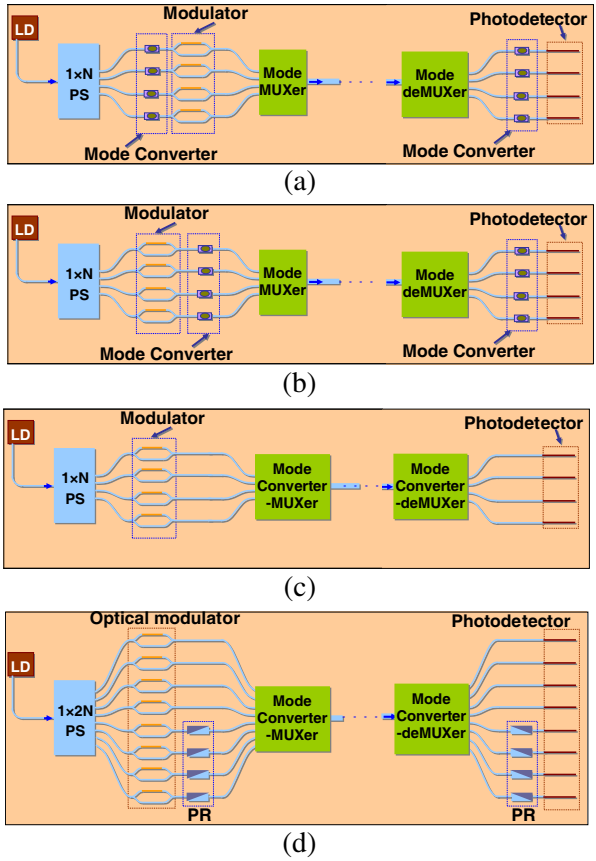

Figure 1. The schematic configuration of a mode-division-multiplexing link, (a) with mode converters, which are inserted in front of the optical modulators, and mode multiplexers; (b) with mode converters, which are inserted between the optical modulators and mode multiplexers; (c) with mode converter-multiplexers after the optical modulators; and (d) with polarization rotators after the optical modulators.

In Fig. 1(a), the continuous-wave light from the LD is uniformly split into N waveguide channels of the fundamental mode by using a regular $1\times N$ power splitter. The fundamental mode of the i-th channel is converted to the i-th higher-order mode by using a mode converter, and then modulated with subsequently cascaded optical modulators. These modulated N-channel data are then multiplexed with a mode multiplexer. At the receiver terminal, the N-channel data are demultiplexed and received by an array of photodetectors. These

optical modulators in this approach have to be designed differently to work for different eigenmodes, which is a big challenge because the optical modulator available currently is designed to operate with the fundamental mode only and it is very hard to be extended to work for higher-order modes.

An improved configuration is to put the optical modulator before the mode converter, as shown in Fig. 1(b), so that the optical modulators can have the same design to work with the fundamental mode, which simplifies the chip design very significantly. Such a configuration has been demonstrated for fiber-based multimode SDM transmission with two channels [27]. In this case mode converters and mode (de)multiplexers are the key components. In Ref. [27], a long-period fiber Bragg grating (LPFBG) is used to realize the LP_{01}-LP_{11} mode conversion and a fiber mode multiplexer based on a symmetrical directional coupler is used by exploiting the difference between the coupling length of the LP_{01} and LP_{11} modes. However, one should note that the scalability of these mode converters as well as mode multiplexers are limited because it is really hard to deal with more than two modes (channels). Therefore, the configuration shown in Fig. 1(b) might not be a good option for a case with more than two channels.

A modified configuration for an optical interconnect link with N multiplexed channels is to use a mode converter-(de)multiplexer, which enables mode conversion and mode multiplexing simultaneously, as shown in Fig. 1(c). The mode converter-(de)multiplexer can be realized by using an evanescent coupling system designed carefully [28–30]. Recently some progress has been made on mode converter-(de)multiplexers based on planar optical waveguides, which will be reviewed below.

When trying to utilize the eigen-modes of both polarizations to form a hybrid multiplexing technology, which enables polarization- and mode-division multiplexing simultaneously to double further the channel number, polarization-handling devices are required, including the PBSs and polarization rotators. Since most of the functional components (e.g., high-speed optical modulators and photodetectors) are polarization-sensitive, one can insert an identical polarization rotator between each optical modulator and the mode multiplexer at the transmitter terminal as well as between the mode (de)multiplexer and each high-speed photodetector at the receiver terminal, as shown in Fig. 1(d). In this approach, one only needs identical optical modulators and identical photodetectors working for one polarization, which make the system design simple and easy. Furthermore, one does not need any polarization rotator working for high-order modes (various polarization

rotators currently available work only for the fundamental mode [5]). Note that the polarization separation/combination with higher-order modes is not easy because a conventional PBS can work for the fundamental modes only and is not available for the present case with multiple modes. A novel multimode PBS is desired to deal with not only the fundamental mode but also the higher-order modes, so that one can realize hybrid multiplexing with doubled channels by making the novel multimode PBS work together with a TE mode multiplexer as well as a TM mode multiplexer.

3. SILICON MULTIMODE PHOTONIC INTEGRATED DEVICES

For a multimode SDM system, in which multiple eigenmodes are involved, any undesired mode conversion/coupling between the mode-channels should be minimized to avoid any significant crosstalk and excess loss. Therefore, it is very essential to understand and evaluate any mode conversion in PICs. As bends and tapers are the most important basic elements for realizing PICs, in Section 3.1 we will give a discussion on light propagation and mode conversion in bent multimode optical waveguides as well as tapered optical waveguides.

On the other hand, a mode converter to realize highly-efficient mode conversion between the eigen-modes is usually desired in order to generate/switch the mode-channel carrying the data in a multimode SDM system. Furthermore, as discussed in Fig. 1, a mode multiplexer is also indispensable and unfortunately it is not easy to realize a mode multiplexer to combine/separate more than two eigenmodes. A mode converter-(de)multiplexer, which can realize mode conversion and mode multiplexing simultaneously, is considered as a better option. Several kinds of structures for mode-(de)multiplexers have been proposed recently, which will be reviewed in Section 3.2.

3.1. Light Propagation and Mode Conversion in Multimode Optical Waveguides

3.1.1. Bent Multimode Optical Waveguides

In order to change the propagation direction of light, we need a bent multimode bus waveguide for a mode-multiplexed optical interconnect link. A small bending radius is usually desired to achieve a compact system. As it is well known, a singlemode SOI strip nanowire enables an extremely sharp bending (∼several microns) with a low loss (including the pure bending loss and the transition loss) due to the ultra-high index contrast [31]. However, for a multimode SOI

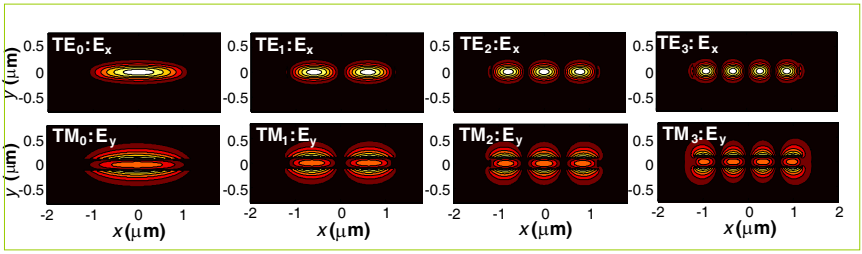

(a)

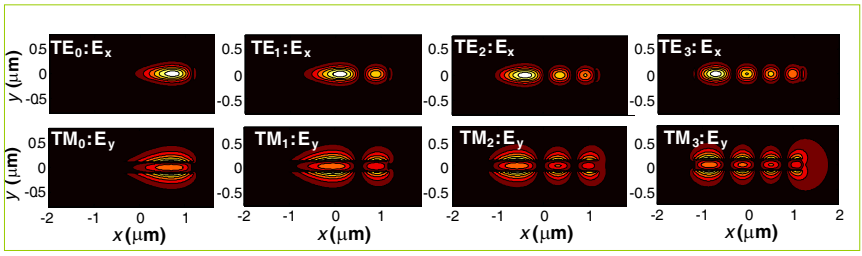

(b)

Figure 2. The field distributions for the eigenmodes in multimode bus waveguides with (a) $R = \infty$ and (b) $R = 10\,\mu$m.

strip nanowire, the modal field is squeezed to the outside sidewall (like a whispery-gallery mode) and becomes very asymmetric when the bending radius becomes small, as shown in Figs. 2(a) and 2(b). As a consequence, when light propagates along a multimode straight waveguide (SWG) connected to a multimode bent waveguide (BWG) with a bending radius R, inter-mode coupling occurs, which introduces large transition loss and mode crosstalk if R is small.

As an example, here we examine the light propagation in a 90° multimode BWG connecting to a multimode SWG and Figs. 3(a)–(d) show the mode excitation ratios of the eigenmodes in the BWG when the input field is the TM_0, TM_1, TM_2, and TM_3 mode of the SWG, respectively. From Figs. 3(a)–(d), it can be seen that the desired intra-mode coupling ratio (from TM_{i_SWG} to TM_{i_BWG}) decreases (due to the increased mode mismatching) while the undesired inter-mode coupling (from TM_{i_SWG} to TM_{j_BWG}, $j \neq i$) increases as the bending radius R decreases. According to the calculation shown in Figs. 3(a)–(d), the undesired inter-mode coupling ratio can be very small (e.g., ~ 0.001 or even smaller) by choosing a large bending radius (e.g., $R = 240\,\mu$m). The insets in Figs. 3(a)–(d) show the simulated light propagation in the structure consisting of a SWG and a BWG with $R = 240\,\mu$m when the input is the TM_0, TM_1, TM_2, or TM_3 modal fields, respectively. From these figures, it can be seen that there is a multimode interference

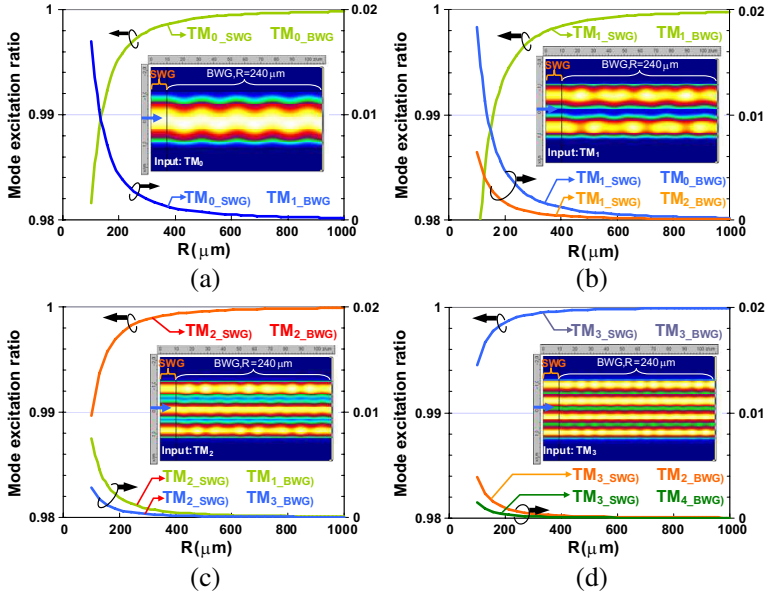

Figure 3. The mode coupling ratios when light is launched from a straight waveguide (SWG) to a bent waveguide (BWG) with a bending radius R. The input fields are the (a) TM, (b) TM_1, (c) TM_2, and (d) TM_3 modal fields of the straight waveguide respectively. Insets: light propagation along the SWG connecting with a BWG.

effect, which indicates that more than one mode is excited as predicted. Therefore, one should be careful in the design of a bent multimode bus waveguide, considering the undesired inter-mode coupling/crosstalk.

In order to achieve a small bending radius as well as low mode crosstalk, one potential method is to reduce the mode mismatching between the SWG and the BWG. In Ref. [26], the refractive index profile of the BWG is modified with the assistance of transformation optics theory so that the bending radius is greatly reduced. Another simple method is to use a bending section whose curvature varies from zero to a certain value (e.g., $1/R_0$) gradually. In this way, the mode of SWG can be converted to the desired mode in the BWG adiabatically. This method has been applied for the design of bent singlemode SOI strip nanowires to suppress significantly both transition loss and inter-mode coupling [32].

3.1.2. Tapered Optical Waveguides

An optical waveguide taper is a fundamental element for PICs to change the light spot size for high coupling efficiency between two

sections with different cross sections [33–40]. For the design of a low-loss taper, one usually makes the taper long enough to be adiabatic so that higher-order modes are not excited [41–44]. This design rule usually works well especially for low index-contrast (Δ) optical waveguides (e.g., SiO_2-on-Si buried optical waveguides). However, it becomes very different for small optical waveguides with very high Δ, e.g., submicron SOI waveguides, which have been used widely for ultra-compact CMOS-compatible PICs [45–56]. For high-Δ optical waveguides, mode conversion between the eigenmodes may occur in an adiabatic tapered structure due to the mode hybridization at some special waveguide widths [57–62]. Here we discuss the light propagation and mode conversion in tapers based on SOI strip nanowires as well as submicron SOI rib waveguides.

3.1.2.1 SOI Strip Nanowire

SOI strip nanowires (as shown in Fig. 4) have been used very popularly for realizing ultrasmall PICs. When the SOI strip nanowire is asymmetrical in the vertical direction (e.g., with an upper-cladding of air), mode conversion between the TM fundamental (TM_0) mode and the first-order TE (TE_1) mode is observed in an adiabatic taper [61, 62] due to the significant mode hybridization at some special values of the waveguide width. The mode hybridization region can be distinguished easily from the calculated dispersion curves shown in Figs. 5(a)–(c) for a SOI strip nanowire with $h_{co} = 220\,\text{nm}$ covered by air ($n_{cl} = 1$), SiO_2 ($n_{cl} = 1.445$), and SiN ($n_{cl} = 2$), respectively. Here the wavelength $\lambda = 1550\,\text{nm}$, the refractive indices of Si and SiO_2 are assumed as $n_{\text{Si}} = 3.455$ and $n_{\text{SiO}_2} = 1.445$, respectively.

For the cases with an upper-cladding of air ($n_{cl} = 1.0$) or Si_3N_4 ($n_{cl} = 2.0$), from Fig. 5(a) or Fig. 5(c) it can be seen that there is a

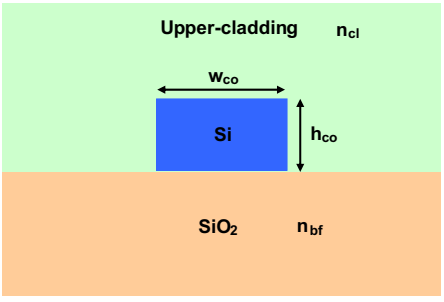

Figure 4. The cross section of an SOI strip nanowire.

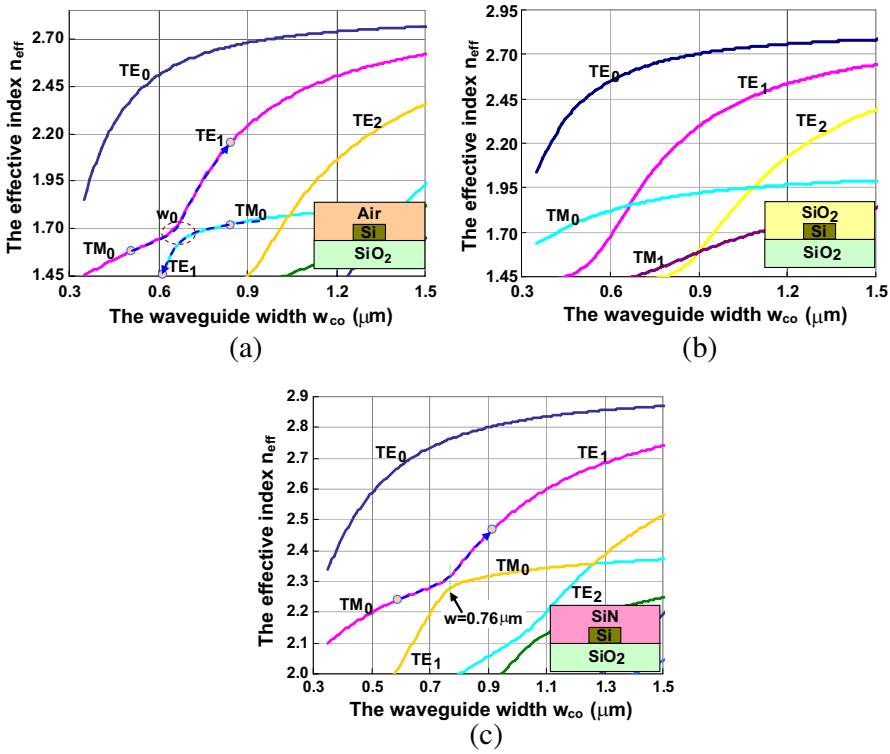

Figure 5. The calculated effective indices for the eigen modes of SOI strip nanowires with the upper-cladding of (a) air, (b) SiO_2, and (c) Si_3N_4. Here the thickness of the Si core layer is $h_{co} = 220\,\text{nm}$.

notable region around $w_{co0} = 0.7\,\mu\text{m}$ or $0.76\,\mu\text{m}$, where the two close curves (corresponding to the TE_1 and TM_0 modes) keep anti-crossing with a small gap between them. This anti-crossing gap around such a special w_{co0} is due to the mode hybridization. In contrast, for the cases with an upper-cladding of SiO_2 (n_{cl}=1.445), no anti-crossing gap exists between any two curves (see Fig. 5(b)). The calculated electrical-field profiles (E_x and E_y) of the two hybridized modes (#1 and #2) when w_{co0}=0.76 μm and $n_{cl} = 2.0$ are shown in Figs. 6(a) and (b) as an example. It can be seen that the amplitudes of the E_x- and E_y-components of the electrical fields are comparable (which is called mode hybridization). In the mode hybridization region, the TE_1 and TM_0 modes are not distinguishable. These two modes will be converted when light propagates along an "adiabatic" (long) taper structure whose end-widths (w_1 and w_2) satisfy the condition: $w_1 < w_{co0} < w_2$.

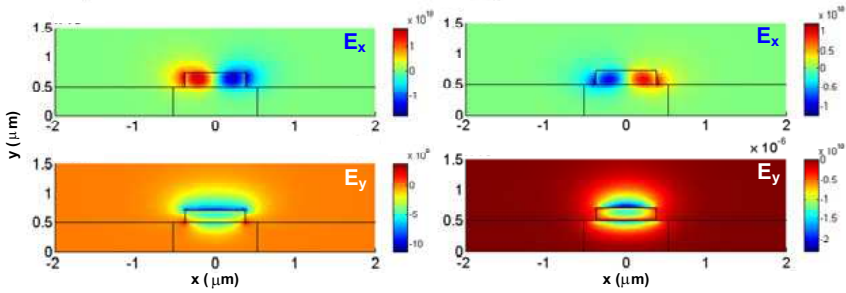

(a) Mode #1: n_{eff}=2.25295 (b) Mode #2: n_{eff}=2.19855

Figure 6. The field profiles for the hybridized modes: (a) $n_{eff} = 2.25295$ and (b) $n_{eff} = 2.19855$. Here the parameters are $w_{co} = 760\,\text{nm}$, $h_{co} = 220\,\text{nm}$, and $n_{cl} = 2.0$.

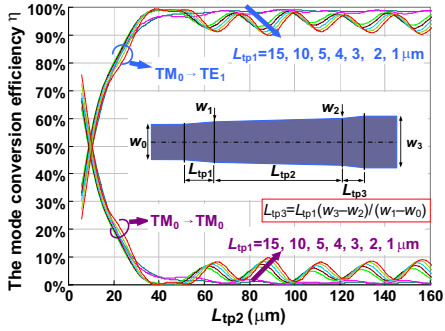

Figure 7. The mode conversion efficiency η (from the TM_0 mode to the TE_1 mode) as L_{tp2} varies when the TM_0 mode is launched. Here the taper length $L_{tp1} = 15$, 10, 5, 4, 3, 2, and 1 μm. The taper length L_{tp3} is given by $L_{tp3} = L_{tp1}(w_3 - w_2)/(w_1 - w_0)$. The other parameters are $w_0 = 0.54\,\mu\text{m}$, $w_1 = 0.69\,\mu\text{m}$, $w_2 = 0.83\,\mu\text{m}$, and $w_3 = 0.9\,\mu\text{m}$. Inset: the schematic configuration of the 3-segment adiabatic taper.

Figure 7 shows the mode conversion efficiencies for the TM_0 mode and the TE_1 mode after the launched TM_0 mode propagates along a waveguide taper. A three-segment taper is used to be compact, as shown in the inset of Fig. 7. The second segment has a very small taper angle to be adiabatic while the first and the third segments are with relatively large taper angles to shorten the whole taper. The end widths (w_1 and w_2) for the second segment are chosen as $w_1 = 0.69\,\mu\text{m}$ and $w_2 = 0.83\,\mu\text{m}$ according to the requirement of $w_1 < w_{co0} < w_2$ (where $w_{co0} = 0.76\,\mu\text{m}$) [62]. The widths ($w_0$, w_3) are chosen as $w_0 = 0.54\,\mu\text{m}$

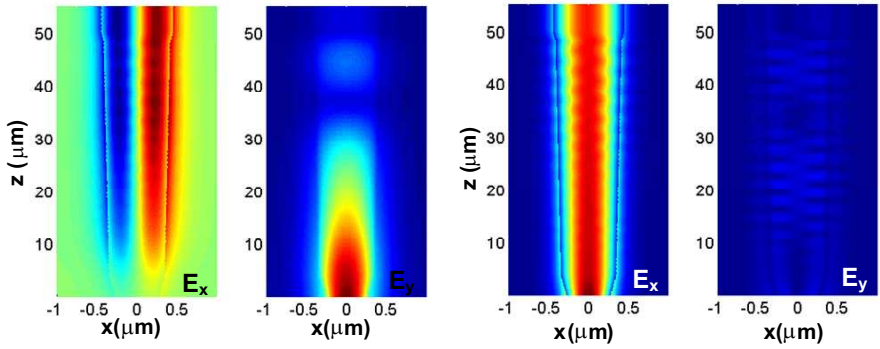

Figure 8. The light propagation in the designed adiabatic taper when the input field is (a) TM polarization, and (b) TE polarization, respectively. Here the taper lengths are: $L_{tp1} = 4\,\mu\text{m}$, $L_{tp2} = 44\,\mu\text{m}$, and $L_{tp3} = L_{tp1}(w_3 - w_2)/(w_1 - w_0)$. The other parameters are $w_0 = 0.54\,\mu\text{m}$, $w_1 = 0.69\,\mu\text{m}$, $w_2 = 0.83\,\mu\text{m}$, and $w_3 = 0.9\,\mu\text{m}$.

and $w_3 = 0.9\,\mu\text{m}$ regarding that a smaller w_0 and a larger w_3 are desired to avoid the mode hybridization at the input section and the output section of the taper. From Fig. 7, one sees that the efficiency can be very high (close to 100%) from the TM_0 mode to the TE_1 mode when choosing the taper length L_{tp2} appropriately for a given taper length L_{tp1}. Fig. 8(a) shows the simulation results for light propagating along the designed taper with $L_{tp1} = 4\,\mu\text{m}$ and $L_{tp2} = 44\,\mu\text{m}$ when the TM_0 mode is launched. In order to give a comparison, the result for the case with the TE_0 mode input is also shown (see Fig. 8(b)). It can be seen that the mode conversion happens for the input TM_0 mode as expected, while there is no mode conversion for the TE_0 mode.

3.1.2.2 Submicron SOI Rib Waveguides

It is well known that submicron SOI rib waveguides are also very popular for silicon integrated optoelectronics [51–56]. One should note that there is a significant difference between an SOI rib waveguide and an SOI strip nanowire. For example, an SOI strip nanowire could be symmetrical or asymmetrical in the vertical direction by simply choosing an appropriate material for the upper-cladding, in which way the mode conversion could be eliminated or enhanced accordingly [62]. However, for an SOI rib waveguide, it is still asymmetrical vertically even when using the same material for the upper- and under-claddings. Therefore, mode conversion may occur between the TM_0 mode and a higher-order

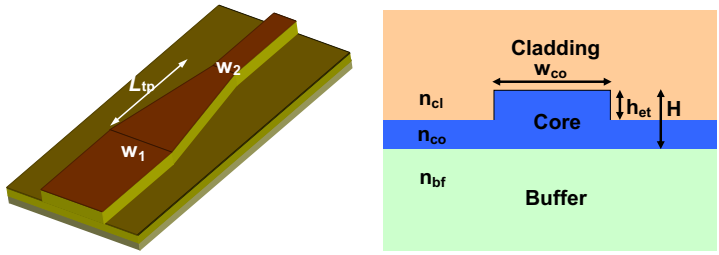

(a) (b)

Figure 9. (a) The schematic configuration of a regular lateral taper; (b) the cross section for an SOI rib waveguide.

TE mode even when using an SOI rib waveguide with the same materials for the upper- and under-claddings. Thus, one must be careful when designing a taper for an SOI rib waveguide. There are two types of tapered structures used very widely. The first one is a regular lateral taper, and the other is the so-called bi-level taper [39, 40, 63, 64].

Figures 9(a)–(b) show the 3D-view of a regular lateral taper and the cross section of a submicron SOI rib waveguide. Figs. 10(a)–(c) show the effective indices for the guided modes of SOI rib waveguides as the core width w_{co} increases when the etching depth is chosen as $h_{et} = 0.4H$, $0.5H$, and $0.6H$, respectively. As an SOI rib waveguide is asymmetrical in the vertical direction, mode hybridization is observed in some special ranges of the rib width, e.g., around $w_{co0} = 1\,\mu$m, and $2.45\,\mu$m, as shown by the circles labeled in Figs. 10(a)–(c). In the region around $w_{co} = 2.45\,\mu$m, the mode hybridization occurs between the TM_0 and the third-order TE (TE_3) mode. The mode profiles of these two modes are shown in Figs. 11(a) and (b), respectively. In contrast, when $w_{co} = 1.0\,\mu$m, the mode hybridization occurs between the TM_0 mode and the first-order TE mode (TE_1), as shown in Figs. 12(a) and (b). Therefore, when the rib width is tapered from $3\,\mu$m to $0.5\,\mu$m, it can be seen that there are two mode-hybridization regions (around $w_{co0} = 1.0\,\mu$m, and $2.45\,\mu$m). Accordingly, we consider the mode-conversion in the two tapers with the following width parameters: (1) w_1=$2\,\mu$m and $w_2 = 2.7\,\mu$m ($w_1 < 2.45\,\mu$m $< w_2$); and (2) $w_1 = 0.8\,\mu$m and $w_2 = 1.5\,\mu$m ($w_1 < 1\,\mu$m $< w_2$).

Figure 13 shows the mode conversion efficiencies coupled to the TM_0 mode and the TE_3 mode after the launched TM_0 mode propagates along the linear lateral taper with $w_1 = 2.7\,\mu$m and $w_2 = 2.0\,\mu$m. From this figure, it can be seen that the conversion efficiency from the TM_0 mode to the TE_3 mode can be very high ($> 90\%$) when choosing the taper length L_{tp} appropriately. For example, when choosing

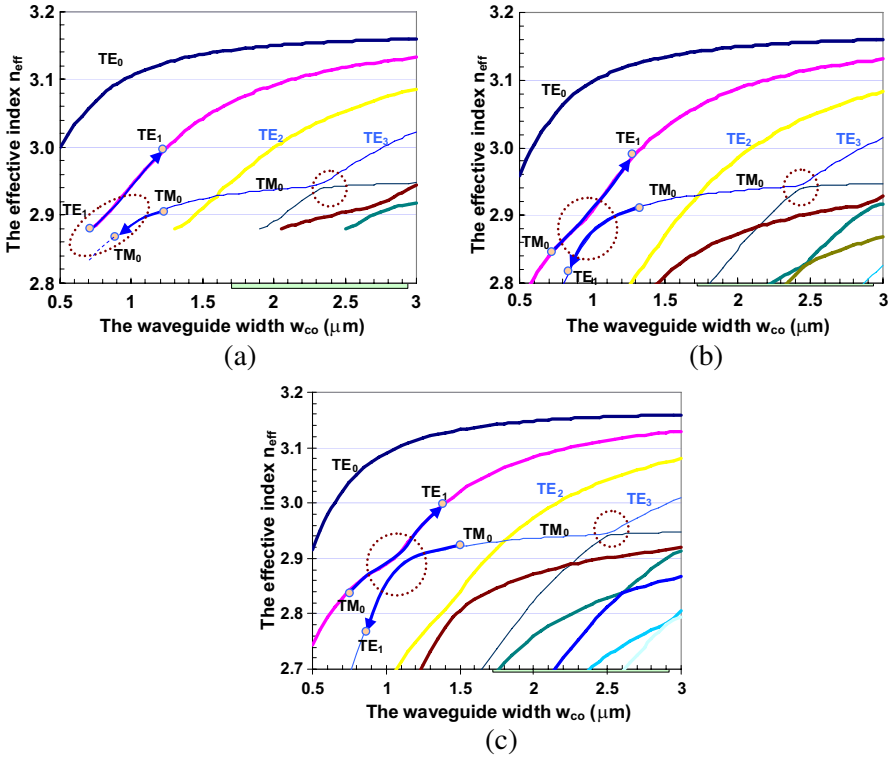

Figure 10. The calculated effective indices for the eigenmodes of an SOI rib waveguide with different values of the etching depth. (a) $h_{et} = 0.4H$, (b) $h_{et} = 0.5H$, and (c) $h_{et} = 0.6H$. Here the total height of the silicon layer is $H = 400\,\text{nm}$.

$L_{tp} = 1500\,\mu\text{m}$, an efficient mode conversion occurs for the case with the TM_0-mode input, as shown by the simulated light propagation given in Fig. 14(a). In contrast, there is no mode conversion when the other mode (e.g., the TE_0, TE_1, and TM_1 modes) is launched, as shown in Figs. 14(b)–(d). When one choose a shorter taper (e.g., 350 μm), the launched TM_0 mode is then converted to the TE_3 mode partially (see Fig. 13) and thus two-mode interference occurs. Such a partial mode conversion should usually be prevented in a multimode SDM system to avoid any significant mode crosstalk. As shown in Fig. 13, the mode conversion could be very small by choosing a very short non-adiabatic taper. For example, for a 10 μm-long taper, the mode conversion from the TM_0 mode to the TE_3 mode is about 5% only and the loss is low acceptably for some applications. The simulated light propagation in

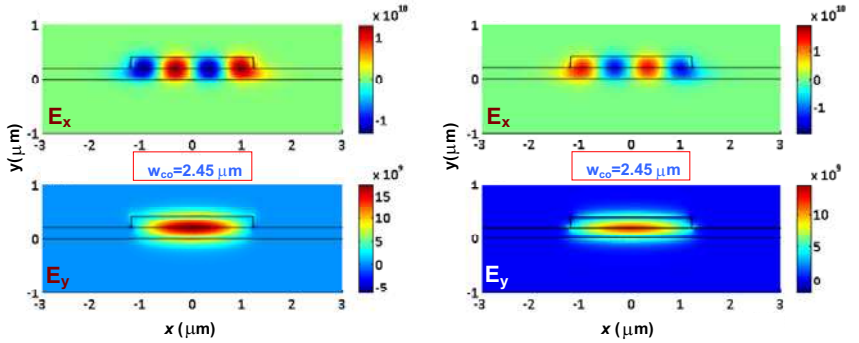

(a) mode #1: n_{eff} =2.942011 (b) mode #2: n_{eff} =2.947892

Figure 11. The field profiles (E_x and E_y) for (a) mode #1 and (b) mode #2 of an SOI ridge waveguide with $w_{co} = 2.45\,\mu\text{m}$. The total height of the Si core layer is $H = 400\,\text{nm}$, and the etching depth $h_{et} = 0.5H$. Here modes #1 and #2 are the two hybridization modes in the region around $w = 2.45\,\mu\text{m}$.

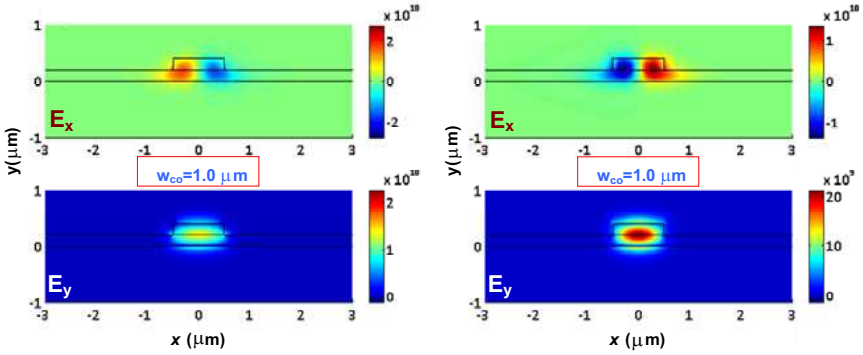

(a) mode #1: n_{eff} =2.908029 (b) mode #2: n_{eff} =2.877179

Figure 12. The field profiles (E_x and E_y) for (a) modes #1 and (b) mode #2 of an SOI ridge waveguide with $w_{co} = 1.0\,\mu\text{m}$. The total height of the Si core layer is $H = 400\,\text{nm}$, and $h_{et} = 0.5H$. Here modes #1 and #2 are the two hybridization modes in the region around $w = 1.0\,\mu\text{m}$.

a 10 μm-long taper is shown in Figs. 15(a)–(d) for the cases with the launched TM_0, TM_1, TE_0, and TE_1 mode fields, respectively. From these figures, it can be seen that more than one mode is excited and some small ripples appear due to the multimode-interference effect.

For a linear lateral taper with $w_1 = 1.5\,\mu\text{m}$ and $w_2 = 0.8\,\mu\text{m}$, there

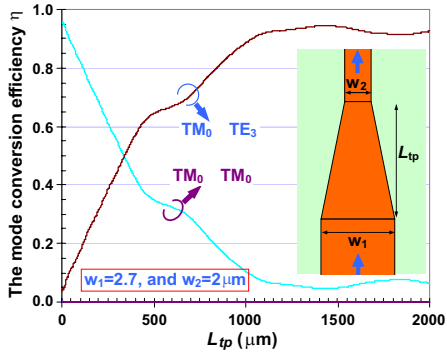

Figure 13. The mode conversion efficiency η as the taper length L_{tp} varies when the TM_0 mode is launched.

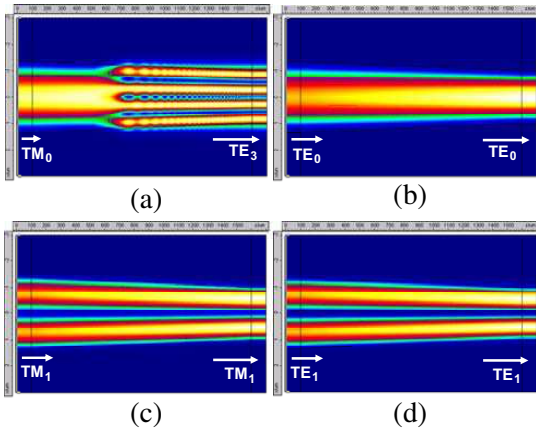

Figure 14. The light propagation in a long taper when the launched field is (a) TM_0, (b) TM_1, (c) TE_0, and (d) TE_1 mode, respectively. The parameters are: $H = 400\,\text{nm}$, $h_{et} = 0.5H$, $w_1 = 2.7\,\mu\text{m}$, $w2 = 2\,\mu\text{m}$, and $L_{tp} = 1500\,\mu\text{m}$.

is a mode hybridization region around $w_{co0} = 1\,\mu\text{m}$ (see Fig. 10(b)), and the mode conversion occurs between the TM_0 mode and the TE_1 mode when the TM_0 mode is launched, as shown in Fig. 16(a). From this figure, it can be seen that the mode conversion efficiency from the TM_0 mode to the TE_1 mode is near 100% when choosing the taper length L_{tp} appropriately. Figs. 16(b) and (c) show the simulated light propagation in a 215 μm-long taper when the TE_0 or TM_0 modal field is launched. It can be seen that the mode conversion occurs for

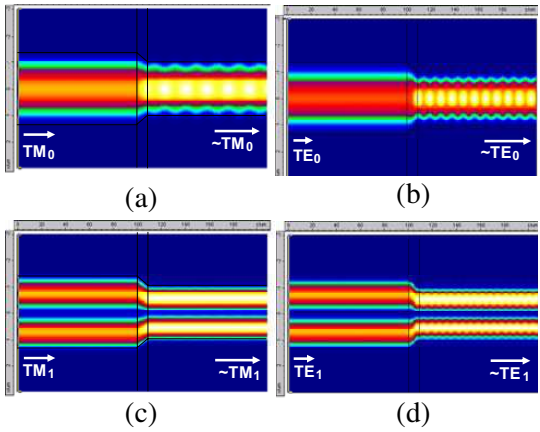

Figure 15. The light propagation in the long taper designed when the launched field is (a) TM_0, (b) TM_1, (c) TE_0, and (d) TE_1 mode, respectively. The parameters are: $H = 400\,\text{nm}$, $h_{et} = 0.5H$, $w_1 = 2.7\,\mu\text{m}$, $w_2 = 2\,\mu\text{m}$, and $L_{tp} = 10\,\mu\text{m}$.

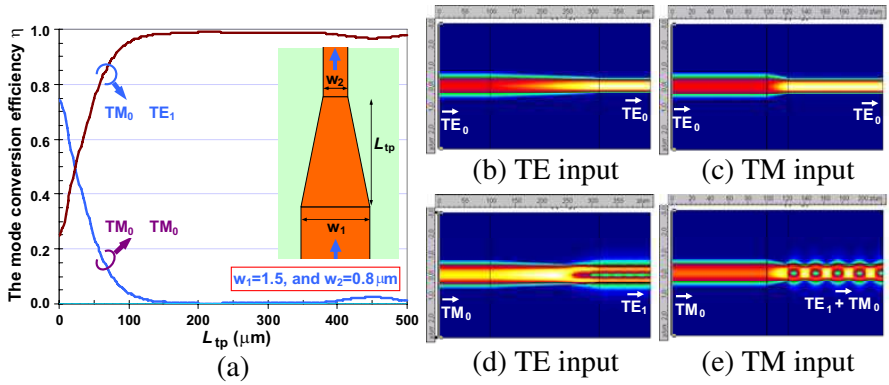

Figure 16. (a) The mode conversion efficiency η as the taper length L_{tp} varies when the TM_0 mode is launched. The parameters are $h_{et} = 0.5H$, $w_1 = 1.5\,\mu\text{m}$, and $w_2 = 0.8\,\mu\text{m}$. Light propagation in the designed taper when the input is the (b) TE_0 modal field, and the (c) TM_0 modal field, respectively, for the cases with the following parameters: $L_{tp} = 215\,\mu\text{m}$, $H = 400\,\text{nm}$, $h_{et} = 0.5H$, $w_1 = 1.5\,\mu\text{m}$, and $w_2 = 0.8\,\mu\text{m}$. Light propagation in the taper when the input is the (d) TE_0 modal field, and the (e) TM_0 modal field, respectively, for the cases with the following parameters: $L_{tp} = 22.4\,\mu\text{m}$, $H = 400\,\text{nm}$, $h_{et} = 0.5H$, $w_1 = 1.5\,\mu\text{m}$, and $w_2 = 0.8\,\mu\text{m}$.

the input TM_0 modal field, while there is no mode conversion for the input TE_0 modal field, as expected. When one chooses a shorter taper, the launched TM_0 mode is partially converted to the TE_1 mode. For example, when L_{tp}=22.4 μm, one has a mode conversion efficiency of 50% from the TM_0 mode to the TE_1 mode, and a significant two-mode interference effect is observed as shown in Fig. 16(d). In particular, when choosing $L_{tp} = 0$ (i.e., without taper), the mode conversion from the TM_0 mode to the TE_1 mode is about 25% and ∼75% power is preserved to the TM_0 mode. A discontinuously tapered structure can be designed to improve the preservation efficiency for the TM_0 mode by further optimizing the widths w_1 and w_2, which is similar to that suggested for the taper design of SOI strip nanowires in Ref. [61].

Such kind of mode conversion has been also observed experimentally in the tapered SOI ridge nanowire shown in Fig. 17(a). The parameters for the tapers are: $h_{rib} = 0.5H$, $H = 400$ nm, $w_1 = 1$ μm, $w_2 = 1.5$ μm, and $w_3 = 3$ μm, and $L_{tp} = 100$ μm. Figs. 17(b)–(c) show the measured light transmissions of a series of taper structures when

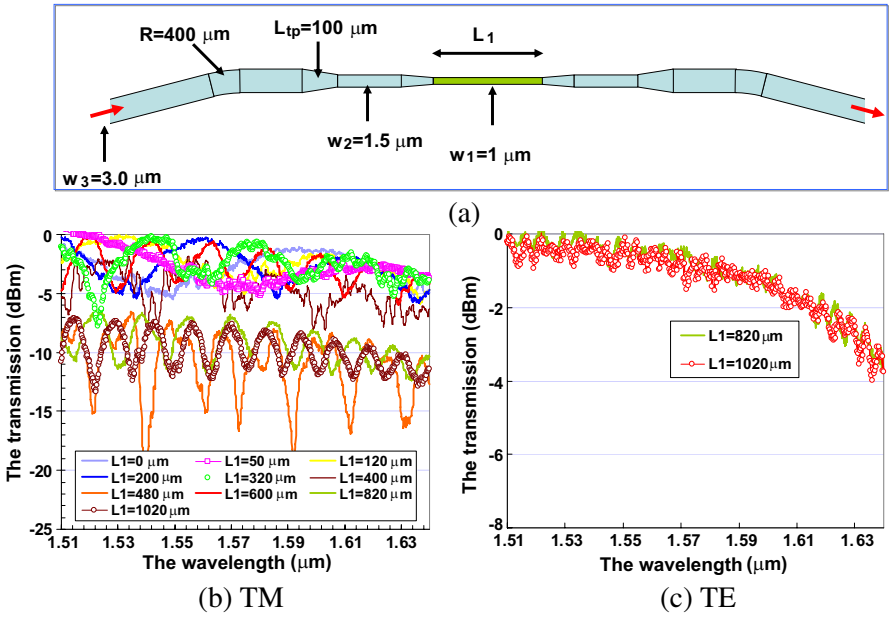

Figure 17. (a) The structure of the lateral taper in our experiments; (b) the measured spectral responses for tapered structures when the TM_0 modal field is launched; (c) the measured spectral responses for tapered structures when the input TE_0 modal field is launched [66].

the TM_0 and TE_0 modes are launched respectively. The length L_1 of the 1 μm-wide straight section in the middle varies from 0 to 1020 μm. From these figures, it can be seen that the spectral response is quasi-periodical for the case with TM-polarization input while there is no quasi-periodical responses for TE-polarization input. This is because some mode conversion between the TM_0 mode and the TE_1 mode occurs in the section tapered from $w_2 = 1.5\,\mu m$ to $w_1 = 1\,\mu m$, which causes two-mode interference phenomena in the 1 μm-wide straight section (see Figs. 16(d)–(e)). From the measurement results shown here, one sees that the mode conversion in a taper structure might be very severe and may influence the performances of optical waveguides and devices. Therefore, one should realize that it is necessary to design the taper very carefully to avoid some undesired mode conversion.

Bi-level taper is another type of tapered structure that has often been used previously to connect two sections with different etching depth [36, 39, 40, 63, 64]. Figs. 18(a) and 18(b) show the 3D-view for the bi-level taper and the cross section for the SOI double-rib waveguide. Usually it is assumed that no higher-order mode is excited when light propagates along a long bi-level taper, so that one achieves a low-loss smooth transition between the fundamental mode of the SOI ridge waveguide and that of the silicon strip waveguide. However, it is found that higher-order modes might be generated even when the taper is long and adiabatic [65]. It is very essential to understand this issue when designing a waveguide taper.

Figures 19(a)–(c) show the effective indices for an SOI double-rib waveguide with $h_{et} = 0.5H$ as the side-rib width w_{side} decreases from 3 μm to 0 when the central-rib width is chosen as $w_{co} = 0.85$, 1, and 1.2 μm, respectively. It is found that the mode hybridization and conversion between the TE_1 mode and the TM_0 mode occur in the

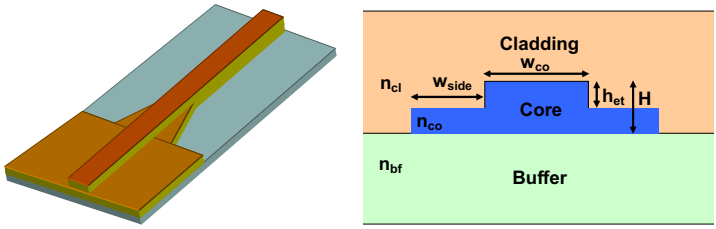

Figure 18. (a) The schematic configuration of a bi-level lateral taper; (b) the cross section for an SOI double-rib waveguide in the taper section.

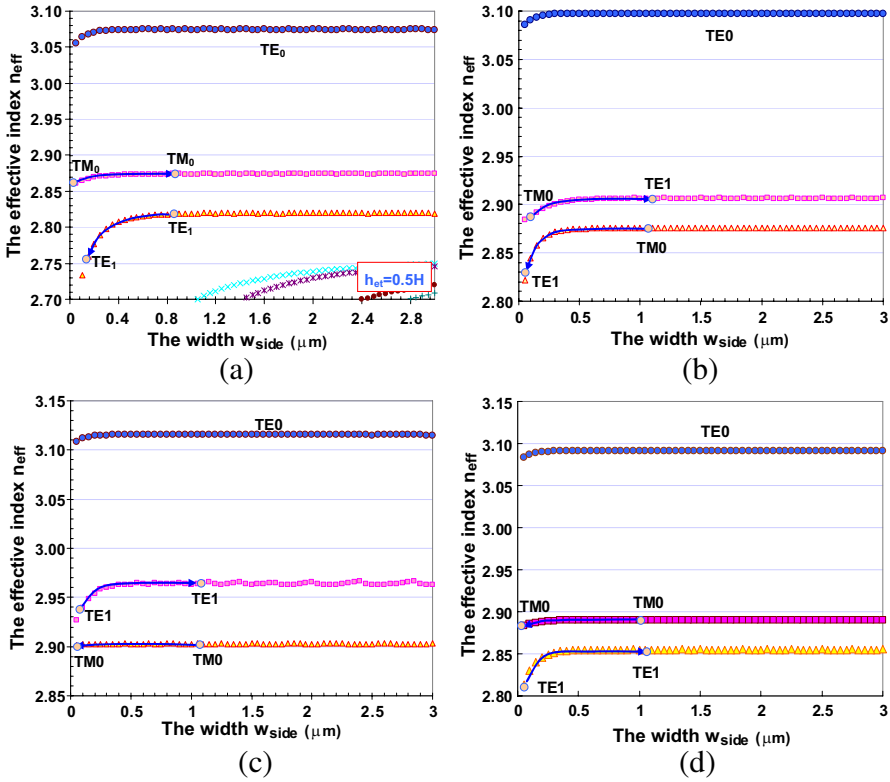

Figure 19. The calculated effective indices for the eigen modes of SOI double-rib waveguides as the side-rib width w_{co} varies with (a) $w_{co} = 0.85\,\mu\text{m}$ and $h_{et} = 0.5H$; (b) $w_{co} = 1.0\,\mu\text{m}$ and $h_{et} = 0.5H$; (c) $w_{co} = 1.2\,\mu\text{m}$ and $h_{et} = 0.5H$; and (d) $w_{co} = 1.0\,\mu\text{m}$ and $h_{et} = 0.6H$. Here $H = 400\,\text{nm}$ [66].

taper when $w_{co} = 1.0\,\mu\text{m}$ according to the dispersion curves given in Fig. 19(b) and the mode profiles shown in Figs. 20(a) and 20(b) for the cases of $w_{side} = 0.5, 0\,\mu\text{m}$. In contrast, there is no mode hybridization and conversion when choosing $w_{co} = 0.85\,\mu\text{m}$ and $1.2\,\mu\text{m}$ according to the results shown in Figs. 19(a) and 19(c) and Figs. 20(a) and 20(b) below. The mode hybridization and conversion can be also avoided by choosing deep etching depth h_{et}, e.g., $h_{et} = 0.6H$ (see Fig. 19(d)).

Figure 21 shows the mode conversion efficiencies from the launched TM_0 mode to the TE_1 mode in a bi-level taper with different lengths for the case of $h_{et} = 0.5H$. From this figure, it can be seen that the mode conversion efficiency from the TM_0 mode to the TE_1 mode is close to 100% when choosing the taper length L_{tp} appropriately (e.g.,

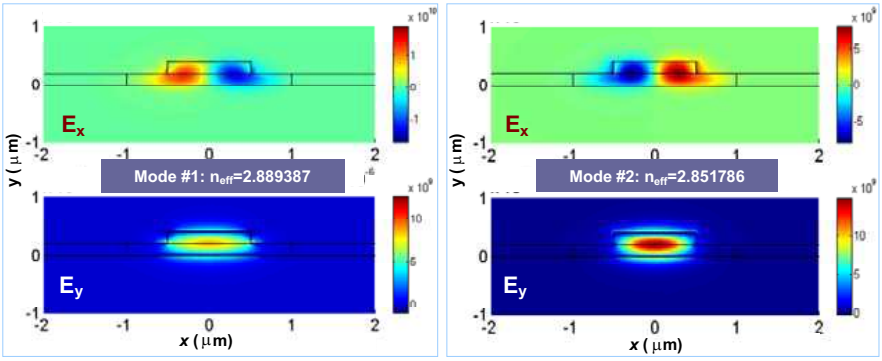

(a) w_{co}=1.0 μm, w_{side}=0.5 μm

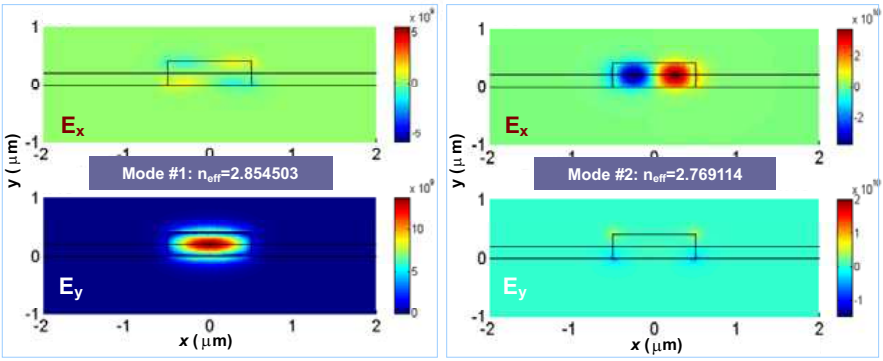

(b) w_{co}=1.0 μm, w_{side}=0 μm

Figure 20. The field profiles (E_x and E_y) for modes #1 and #2 of a double ridge waveguide with: (a) $w_{side} = 0.5\,\mu m$; (b) $w_{side} = 0$. The other parameters are: $w_{co} = 1\,\mu m$, $H = 400\,nm$, and $h_{et} = 0.5H$. Here modes #1 and #2 are the two lowest order modes when excluding the TE_0 mode.

$> 300\,\mu m$). Figs. 22(a)–(c) show the simulated light propagation in the designed taper with $L_{tp} = 300\,\mu m$ when the TM_0, TE_1 or TE_0 modal field is launched respectively. It can be seen that the TM_0 mode and TE_1 mode are converted to each other very efficiently while no mode conversion is observed for the launched TE_0 modal field. The mode conversion between such a pair of eigenmodes can be useful for a mode multiplexed optical interconnect to realize the data exchange between two mode-channels.

As discussed above, according to Figs. 19(a)–(d) it can be seen that the mode conversion between the TM_0 mode and the higher-order TE mode could be avoided or enhanced by choosing the rib width or

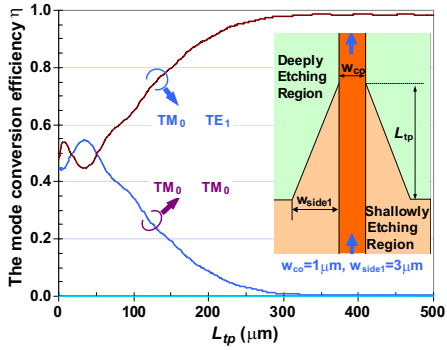

Figure 21. The mode conversion efficiency η as L_{tp} varies when TM_0 modal field is launched. The parameters are $w_{co} = 1.0\,\mu m$, $w_{side} = 3.0\,\mu m$, and $h_{et} = 0.5H$ [66].

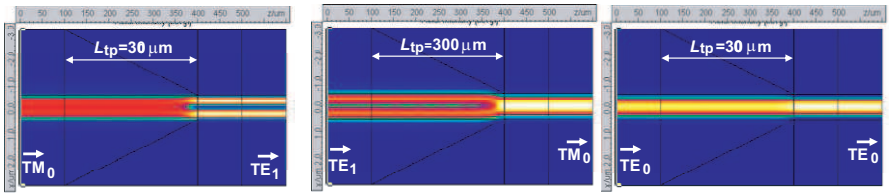

(a) TM input (b) TE_1 input (c) TE input

Figure 22. The light propagation in the taper when the input field is (a) TM_0, (b) TE_1, and (c) TE_0 respectively. The parameters are: $H = 400\,nm$, $h_{et} = 0.5H$, $w_{co} = 1.0\,\mu m$, and $L_{tp} = 300\,\mu m$.

etching depth appropriately. For example, the mode conversion could be avoided when choosing a relatively deep rib, e.g., $h_{et} = 0.6H$, as indicated in Fig. 19(d), which is verified by the measured light transmissions shown in Figs. 23(a) and (b) for straight waveguides with bi-level tapered structures at the input/output ends. There is no notable periodical ripple observed for the measured spectral response, which indicates that no mode conversion occurs as the theoretical calculation predicted.

In summary, for a regular lateral taper whose width ranges from w_1 to w_2 ($w_1 < w_2$), the mode conversion between the TM_0 mode and higher-order TE modes (e.g., TE_1, TE_3) occurs when there is a mode hybridization region in the range of $w_1 < w < w_2$ according to the simulation given above. Such a mode conversion could be very efficient (close to 100%) when the taper length is long enough, which

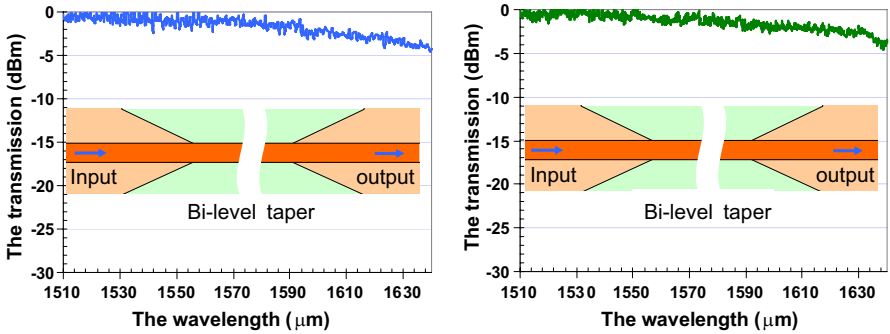

Figure 23. The measured spectral responses for bi-level tapered structures when the input is (a) the TE_0 modal field; (b) the TM_0 modal field; The parameters are: $H = 400\,\text{nm}$, $w_{co} = 1\,\mu\text{m}$, $H = 400\,\text{nm}$, and $h_{et} = 0.6H$ [66].

is very useful for achieving low-loss data-exchange between two mode-channels in a mode multiplexing system. On the other hand, it is also possible to design a taper to minimize the mode conversion by choosing the etching depth (h_{et}) or the taper end-widths (w_1 and w_2) when it is desired to achieve a low-loss and low-crosstalk waveguide taper, which is a very important basic element for many photonic integrated circuits.

3.2. Mode Converter-multiplexer

As discussed in Section 2, a mode converter plays an important role as a key component in a mode-division multiplexed system to achieve highly-efficient mode conversion between two eigen-modes. Several approaches have been proposed for the mode conversion between the fundamental mode and a desired higher-order mode. For free space optics, the desired mode is excited by the LP_{01} mode using transverse-mode matched method with a phase management at the expense of the bulky volume [16–19]. For a fiber based converter, a long-period fiber grating (LPFG) has been proposed earlier to realize the LP_{01}-LP_{11} mode conversion [20–23]. The mode converter can also be realized by the evanescent coupling based on the phase matched condition for a fiber with two asymmetric cores [66, 67] or a few cores [68, 69]. And a structure of "photonic-lantern" can also realize mode conversion by an adiabatic taper [70]. However, it would be easier to realize mode conversion for PICs rather than the fiber case due to the convenient and precise fabrication. Grating couplers have been proposed and demonstrated to synthesize the desired field profiles and excite a few

LP fiber modes by vertical selective mode coupling [71–74]. In Ref. [25], an SiO_2-on-Si asymmetric mode coupler is utilized to convert the LP_{01} to the LP_{11} mode and the waveguides are connected to the few-mode fiber by butt coupling method. In Ref. [75], a $\sim 18\,\mu$m-long on-chip mode converter is demonstrated with a Mach-Zehnder interferometer (MZI) to realize the mode conversion between the "zero-th" and first-order optical modes. However, this is hard to be extended for realizing the mode conversion from the fundamental mode to a desired higher-order mode. Even when mode conversion can be realized, one should note that it is still not easy to make a mode multiplexer to combine the fundamental mode and the higher-order modes together.

A more concise approach is to use a mode converter-multiplexer which can achieve the mode conversion and mode multiplexing simultaneously, as shown in Fig. 1(c). Several kinds of structures for mode converter-(de)multiplexer have been proposed. In [76], a design based on multi-mode interference is proposed, but works for two mode-channels only and is not easily extendable for more mode-channels. Adiabatic mode-evolution couplers have also been proposed to realize mode (de)multiplexing by using directional couplers [77–79] or Y-junctions [80–86], which can be extended to handling with more mode-channels. In Refs. [77, 78], a mode add-drop multiplexer based on an adiabatic directional-coupler is designed with 1 μm-thick SOI ridge waveguides and the device length is more than 1 mm. The length of an adiabatic directional-coupler can be shortened when using smaller SOI optical waveguides. For example, recently a $\sim 300\,\mu$m-long two-channel mode (de)multiplexer based on adiabatic couplers was demonstrated by using 340 nm-thick SOI nanowires to combine/separate two supermodes in a bus waveguide with two cores [79]. Y-junctions provide another attractive option to realize mode-conversion/(de)multiplexing [80–86]. In Ref. [80], the concept of two-mode (de)multiplexing in asymmetric Y-branches is generalized to several mode-channels and some important design rules were given. With this concept, mode-order converters in a multimode waveguide were designed and presented [81, 82]. In Ref. [84], a $\sim 1\,$cm-long Y-junction based on weakly-confined optical waveguides was designed to realize mode (de)multiplexing with four modes. Recently, a two-channel mode multiplexer was demonstrated experimentally by using an asymmetric Y-junction based on SOI nanowires [85]. The Y-junction can be also cascaded in series to handle more mode channels [86]. These devices based on adiabatic mode-evolution couplers usually suffer from the large footprints [87].

According to the coupled mode theory, an efficient mode conversion can be achieved between the eigen-modes in different

optical waveguides when the phase matching condition is satisfied. Asymmetrical directional couplers (ADCs) consisting of different optical waveguides have been used successfully for polarization beam splitters [88, 89]. Particularly, in Ref. [88] the coupling between the TM_0 mode in a narrow input waveguide and the TM_1 mode in a wide middle waveguide is utilized to realize a PBS based on a three-waveguide-coupling system. Generally speaking, an ADC consists of a narrow access waveguide (w_a) and a wide bus waveguide (w_b) to form an evanescent coupling region, as shown in Fig. 24(a). Their widths (w_a and w_b) are chosen according to the phase matching condition, i.e., $n_{eff0}(w_a) = n_{effi}(w_b)$, where $n_{eff0}(w_a)$ and $n_{effi}(w_b)$ are the effective indices of the fundamental mode of the narrow access waveguide and the i-th higher-order mode of the bus waveguide, respectively. In this way, the fundamental mode of the narrow access waveguide can be coupled to the desired i-th higher-order mode in the bus waveguide completely. On the other hand, those undesired eigen-modes will hardly be excited due to the significant phase mismatching so that the crosstalk between the mode-channels is low in principle.

Therefore, it can be seen that an ADC provides a good approach to generate a desired higher-order mode. With ADCs, one can realize a mode converter-(de)multiplexer [27, 89, 90], which is scalable and flexible to excite any desired high-order mode. In Ref. [27], we have previously proposed and demonstrated a 4-channel silicon mode converter-multiplexer operating for TM polarization with low loss, low crosstalk as well as small footprint. Recently a grating-assist ADC was designed to construct a 4-channel narrow-band mode converter-multiplexer [28]. In Ref. [29], a three-channel converter-multiplexer combining ADCs and microrings for simultaneous mode- and wavelength-division-multiplexing has also been recently realized to expand the link capacity.

An ADC is designed according to the phase matching condition and the dispersion curves shown in Fig. 24(b) for an SOI strip nanowire with, e.g., $h_{co} = 220\,\text{nm}$. For example, the narrow access waveguides are designed to have the same width $w_a = 0.4\,\mu\text{m}$ while the corresponding optimal widths for the bus waveguide are chosen as $w_1 = 1.02\,\mu\text{m}$, $w_2 = 1.68\,\mu\text{m}$, and $w_3 = 2.35\,\mu\text{m}$ for the first, second and third higher-order TM modes, respectively [27]. The optimal lengths for the coupling regions are determined as $L_{c1} = 4.5\,\mu\text{m}$, $L_{c2} = 7.0\,\mu\text{m}$, and $L_{c3} = 9.7\,\mu\text{m}$ with a 3D-FDTD simulation when the gap width $w_g = 0.3\,\mu\text{m}$. Figs. 24(c)–(e) shows the simulated light propagation in the designed ADCs. It can be seen that an efficient mode conversion is achieved from the TM_0 mode in the narrow access-waveguide to the desired higher-order mode in the wide bus-waveguide,

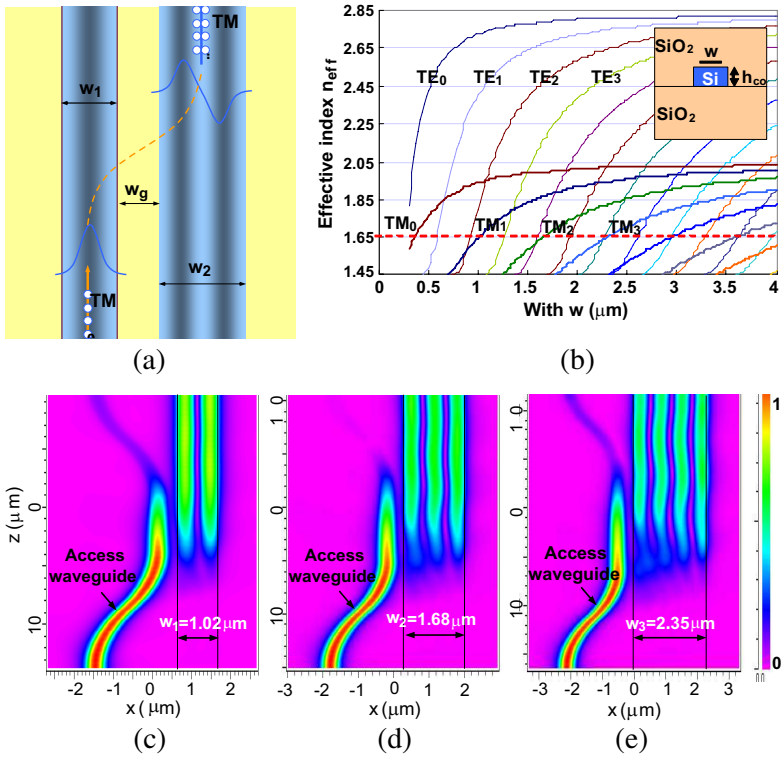

Figure 24. (a) The calculated effective indices of the guided-modes in an SOI strip nanowire with $h_{co} = 220\,\text{nm}$; (b) an asymmetrical directional coupler; The FDTD simulated light propagation in the designed i-th stage ADC with (c) $i = 1$, (d) $i = 2$, and (e) $i = 3$.

with very little power left in the access waveguide. The theoretical excess loss of the designed ADCs is almost zero ($< 0.1\,\text{dB}$) and the channel crosstalk at the central wavelength is also very low ($< -25\,\text{dB}$).

The ADCs can be then conveniently cascaded to realize a mode converter-multiplexer to combine N mode-channels. In Refs. [14, 27], a $1 \times N$ ($N \geq 4$) mode converter-(de)multiplexer consisting of cascaded ADCs based on thin SOI strip nanowires (e.g., $h = 220\,\text{nm}$) was proposed and demonstrated, as shown in Fig. 25(a). The bus waveguide consists of N straight segments whose widths are different and an adiabatic taper is inserted between the adjacent two straight segments. Figs. 25(b)–(e) show the simulated light propagation in the designed 1×4 mode-multiplexer when light is launched from different input ports. From Figs. 25(b)–(e), it can be seen that the desired

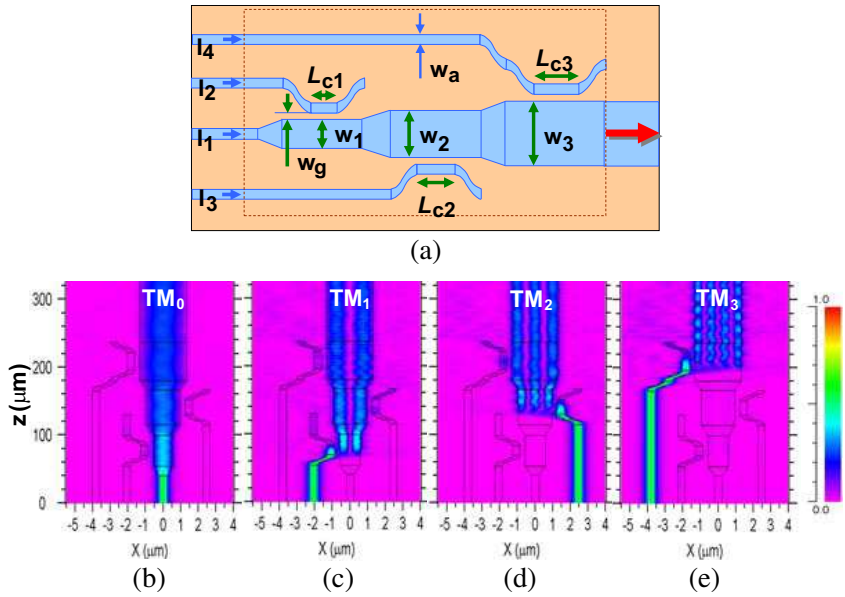

Figure 25. (a) The schematic configuration of the mode converter-multiplexer with 4 channels; The simulated light propagation in the designed mode converter-(de)multiplexers with the light launched at (b) input 1; (c) input 2; (d) input 3; and (e) input 4.

higher-order mode in the bus waveguide is excited efficiently and all the four channels are multiplexed very well in the bus waveguide when light goes through the 1×4 mode-demultiplexer, as predicted. According to the reciprocity of light, one can realize a mode converter-demultiplexer easily.

In order to characterize a mode convert-(de)multiplexer, one usually needs a PIC including a mode multiplexer (with input ports $I_1 \sim I_4$), and a mode demultiplexer (with output ports $O_1 \sim O_4$), as shown in Fig. 26(a). The simulated light propagation in the designed PIC when all the input ports are fed with the TM_0 mode is shown in Fig. 26(b). Since there are four eigenmodes excited in the multimode bus waveguide, multimode interference occurs as shown in Fig. 26(b). Note that this kind of multimode interference does not introduce any channel-crosstalk because these modes are orthogonal to each other. From this figure, it can be seen that the four mode-channels are multiplexed/demultiplexed very well.

Figure 26(c) shows the SEM (scanning electron microscope) picture for the chip fabricated with the regular processes for

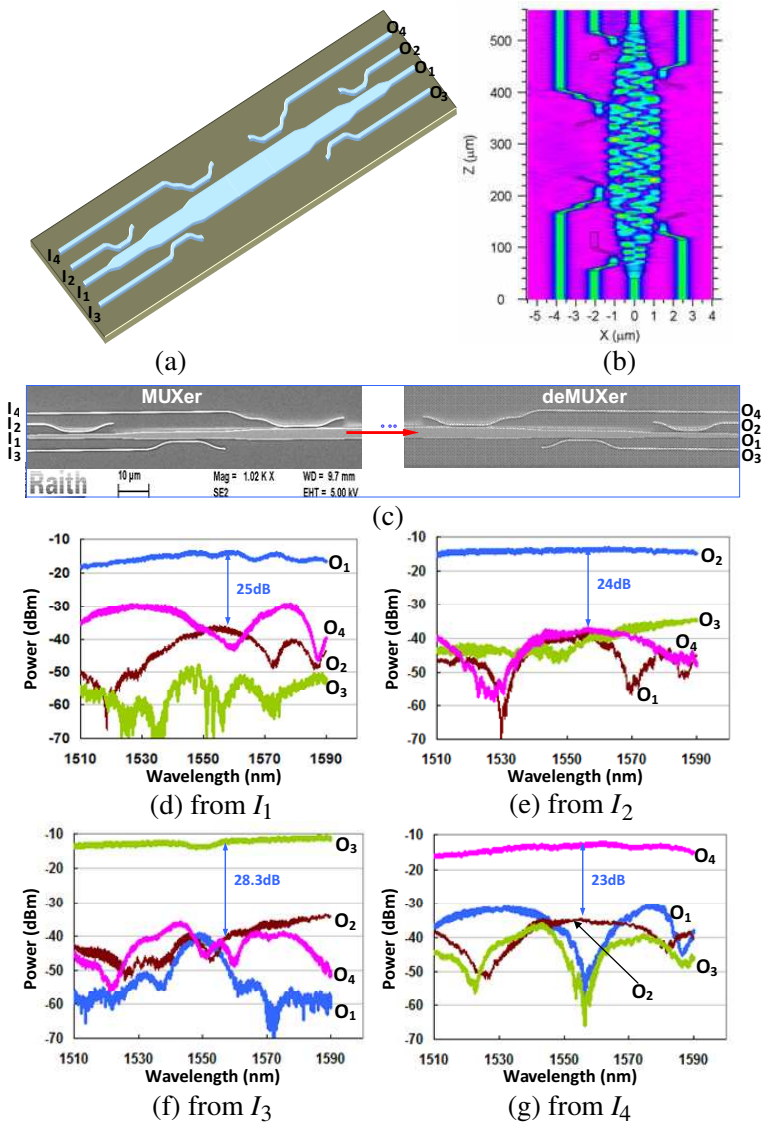

Figure 26. (a) The silicon PIC including a mode converter-multiplexer, the multimode bus waveguide and a mode converter-demultiplexer. (b) The simulated light propagation in the designed structures with all inputs. (c) The SEM picture for the 4×1 mode multiplexer and 1×4 mode demultiplexer integrated on the same chip; (d) The measured responses at output ports (O_1, O_2, O_3, and O_4) when light is input from the port of (d) I_1, (e) I_2, (f) I_3, and (g) I_4.

silicon photonics including an E-beam lithography process, an inductively-coupled plasma dry etching process for silicon, and a PECVD deposition process for 1 µm-thick SiO_2 upper-cladding layer. Figs. 26(d)–(g) show the measured transmission responses at all output ports O_1, O_2, O_3, and O_4 when light is input from port I_1, I_2, I_3, and I_4 respectively. From these figures, it can be seen that one has the maximal output from the j-th input port to the j-th output port as desired. The fabricated device has a low excess loss (< 0.5 dB) and low crosstalk (< -20 dB) over a broad band around the central wavelength. The total insertion loss of about $12 \sim 13$ dB is mainly from the butt-coupling loss between the fiber and the chip, which can be reduced by introducing grating couplers [91] or inversed tapers [92].

The link capacity with single-wavelength light carrier can be improved further by combining the multimode SDM and PDM technologies, which doubles the link capacity. In this situation the key is to design the hybrid (de)multiplexer to combine multiple eigenmodes for both polarizations at the transmitter/receiver end. In principle, this can also be achieved by cascading mode multiplexers and a PBS with the ability to deal with higher-order modes for both polarizations. However, as discussed in Section 2, almost all the conventional PBSs work for only the fundamental modes of TE and TM polarizations and the PBS working for the multimode case is a challenge. Fig. 27 shows a design to realize a hybrid (de)multiplexer enabling mode-/polarization-division-(de)multiplexing simultaneously [93]. A PBS is used to combine/separate the TE_0 and TM_0 modes while the high-order modes (TE_1, TE_2, TE_3, TM_1, TM_2, and TM_3) are (de)multiplexed by using six cascaded ADCs. The PBS is achieved by using a three-waveguide coupler [87], which is optimally designed according to the phase matching condition for the TM polarization modes.

Basically the ADCs for six higher-order modes are designed according to the phase-matching condition as shown in Ref. [93]. However, the hybrid multiplexer has to handle multiple eigenmodes for

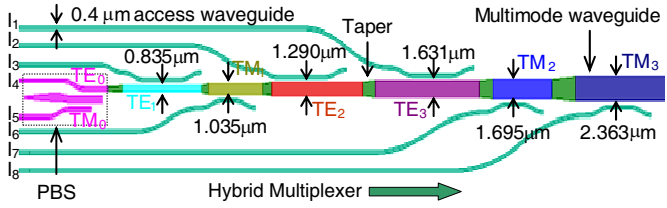

Figure 27. A 8-channel hybrid multiplexer enabling mode- and polarization-division-(de)multiplexing simultaneously [93].

two polarizations and consequently the situation becomes complicated. One has to check the channel crosstalk from mode-channels of both polarizations carefully. For example, for the ADC (with $w_b = 1.272\,\mu\text{m}$ and $w_a = 0.4\,\mu\text{m}$) designed for the TE_2 mode, the phase mismatch between the TM_1 mode in the bus waveguide and the TM_0 mode in the access waveguide is not large. Consequently there is partial coupling between the TM_1 mode in the straight bus section and the TM mode in the access waveguide, which will cause some excess loss and some crosstalk from the TM_1 mode channel to the TE_2-mode channel. In order to solve this problem, the width of the access waveguide is modified slightly to be $w_a = 0.406\,\mu\text{m}$ so that the length L_c of the coupling region can be chosen as $L_c = L_{\pi\_\text{TE2}} = 4L_{\pi\_\text{TM1}}$, in which L_{π_TE2} and L_{π_TM1} are the beat lengths for the TE_2 mode and the

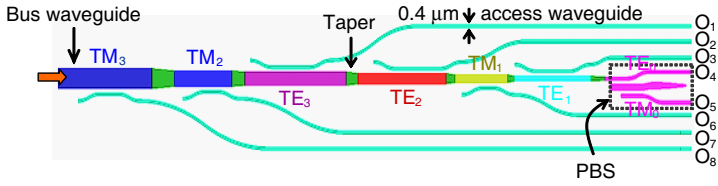

Figure 28. The schematic configuration of the 8-channel hybrid demultiplexer for the simulation.

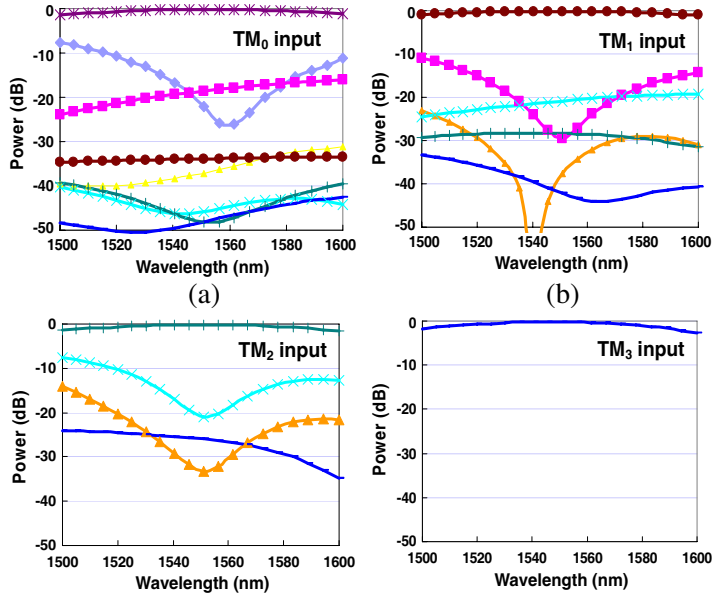

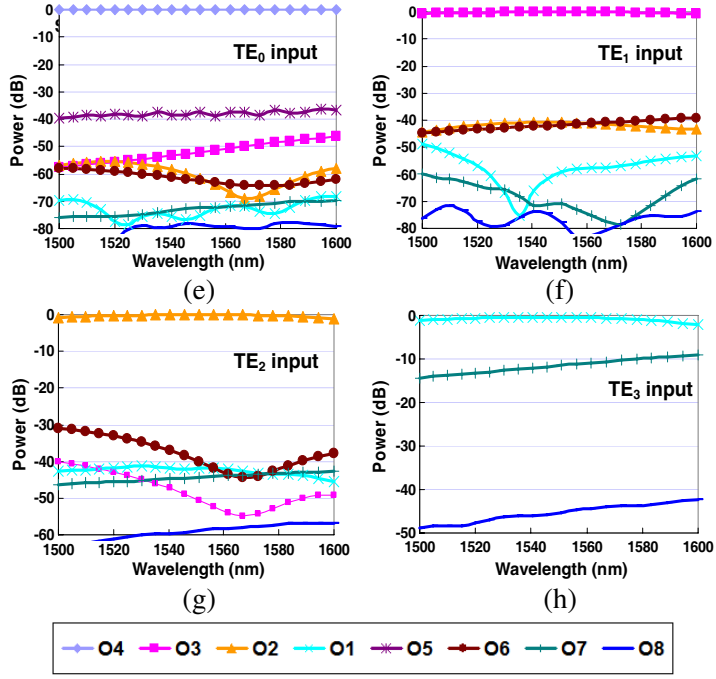

Figure 29. The simulated performance of the 8-channel hybrid demultiplexer with $\Delta w = 0$ nm when input field is of (a) TM_0, (b) TM_1, (c) TM_2, (d) TM_3, (e) TE_0, (f) TE_1, (g) TE_2, and (h) TE_3 mode.

TM_1 mode, respectively. This way the excess loss and crosstalk can be reduced greatly.

In order to evaluate theoretically the mode-channel crosstalk of the (de)multiplexer, the transmissions of the present hybrid demultiplexer (see Fig. 28) is calculated as shown in Fig. 29. In this calculation, each power-normalized guided-mode is launched at the bus waveguide separately and the power at each output port is monitored. It is noted that some higher-order modes launched will become cut-off as it propagates along the bus waveguide (which is tapered down). The powers monitored at some of the undesired output ports are very low intrinsically. In this case, the curves are not shown in the figures. For example, when the TM_3 mode is launched, the power is mainly dropped by the first ADC and output from port O_8 (as shown in Fig. 28). The residual TM_3 mode in the bus waveguide will be leaky because the TM_3 mode is not supported in the following bus waveguide that has been tapered down. As a consequence, the crosstalk (i.e., the power received at the other ports $O_1 \sim O_7$) is very low and the curves are not given in

Fig. 29(d). From these figures, it can be seen that around the central wavelength 1550 nm the crosstalk from the TE_3 mode to the TM_2 mode is relatively the largest (~ -11 dB) and a bit wavelength-dependent. This is because the ADC working for the TM_2 mode almost satisfies the phase matching condition for the TE_3 mode. This crosstalk is a kind of polarization crosstalk, which can be removed by using a TM-pass polarizer or PBS in the present case. It should also be noted that the crosstalk is not reciprocal and the crosstalk from the TM_2 mode to TE_3 mode channel is much lower because the TM_2 mode is dropped before it arrives at the ADC working for the TE_3 mode and little power of the TM_2 mode is left in the bus waveguide to influence (i.e., give some crosstalk to) the TE_3 mode channel.

The fabrication tolerance of the present hybrid demultiplexer is also analyzed by assuming that the present hybrid demultiplexer has a waveguide-core width variation of $\Delta w = +10$ nm and -10 nm, as shown in Figs. 30(a)–(h), and Figs. 31(a)–(h), respectively. From the figures, it can be seen that the present hybrid demultiplexer has nice fabrication tolerance of about ± 10 nm. The crosstalk for all the channels are lower than -10 dB over a broad band even when $\Delta w = +/-10$ nm. At the central wavelength around 1550 nm, the crosstalk is as low as -15 dB (except the TE_3 mode-channel).

Figures 32(a)–(h) show the calculated excess loss of the 8 mode-channels with $\Delta w = +/-10$ nm. It can be seen that the excess

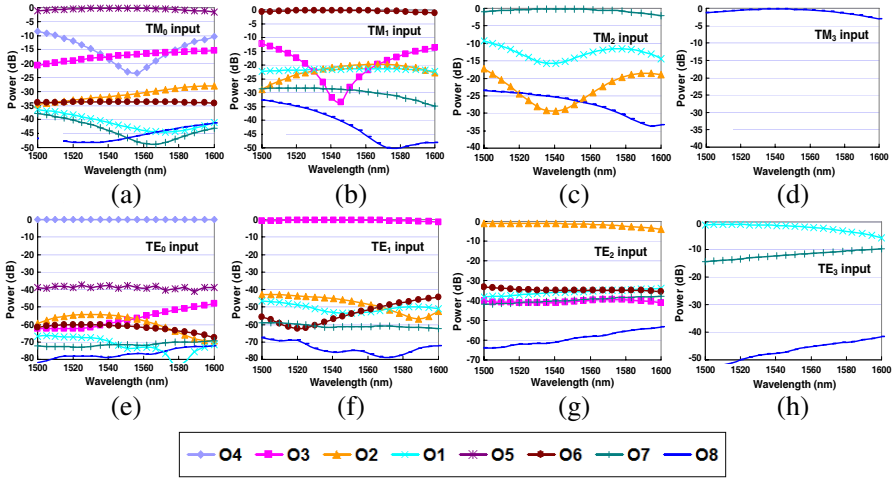

Figure 30. The simulated performance of the 8-channel hybrid demultiplexer with $\Delta w = +10$ nm when the input field is of (a) TM_0, (b) TM_1, (c) TM_2, (d) TM_3, (e) TE_0, (f) TE_1, (g) TE_2 and (h) TE_3 mode.

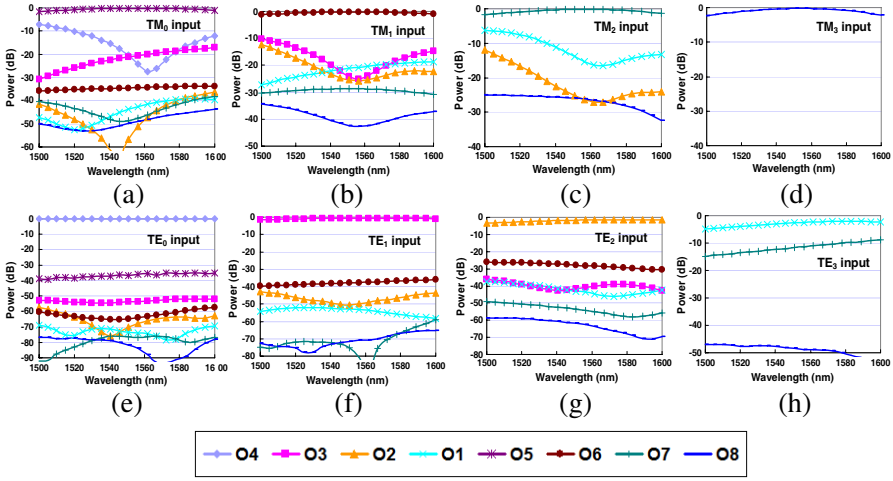

Figure 31. The simulated performance of the 8-channel hybrid demultiplexer with $\Delta w = -10$ nm when input field is of (a) TM_0, (b) TM_1, (c) TM_2, (d) TM_3, (e) TE_0, (f) TE_1, (g) TE_2 and (h) TE_3 mode.

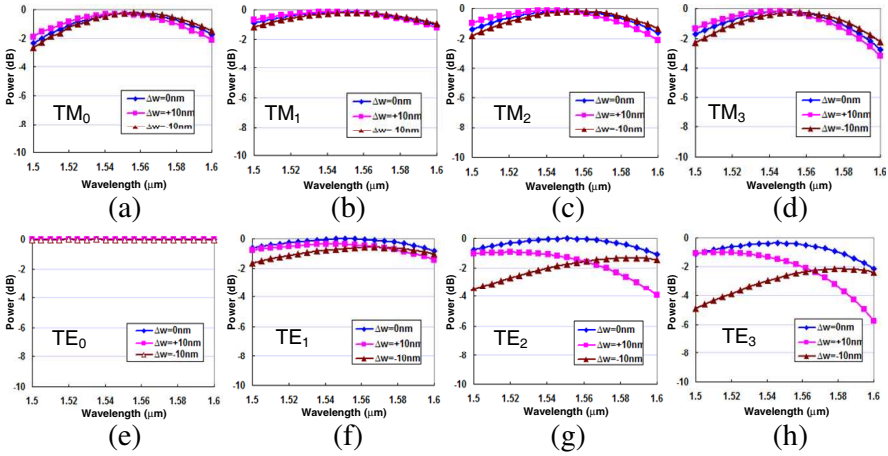

Figure 32. The calculated excess loss for the 8-channel hybrid demultiplexer with $\Delta w = 0, \pm 10$ nm for the mode channel of (a) TM_0, (b) TM_1, (c) TM_2, (d) TM_3, (e)TE_0, (f) TE_1, (g) TE_2 and (h) TE_3.

losses for the TM_0, TM_1, TM_2, TM_3, TE_0, and TE_1 mode-channels are not sensitive to variation Δw. However, for the TE_2 and TE_3 mode-channels, the excess loss around the central wavelength 1550 nm increases by $2 \sim 3$ dB when $\Delta w = +/-10$ nm, as shown in Figs. 32(g)–

(h) (the excess loss increase will be less than 1 dB when $|\Delta w| < 5$ nm).

In summary, the present hybrid demultiplexer can tolerate the fabrication error of $\Delta w = \pm 5 \sim 10$ nm regarding the requirements of the crosstalk < -10 dB and the excess loss < 2 dB. This makes the fabrication of the present hybrid demultiplexer feasible with the advanced nano-fabrication technology available today.

Figure 33 shows the optical image of the fabricated PIC consisting of an 8-channel hybrid multiplexer (with input ports $I_1 \sim I_8$), a 2.36 μm-wide and 100 μm-long multimode bus waveguide, and a hybrid demultiplexer (with output ports $O_1 \sim O_8$). Figs. 34(a)–(h) show the measured transmission responses at all output ports ($O_1 \sim O_8$) when light is launched at input ports $I_1 \sim I_8$ respectively. Here the TE_0 mode of the access waveguide is launched at ports $I_1 \sim I_4$ while the TM_0 mode is launched at ports $I_5 \sim I_8$. According to the normalization with respect to the transmissions of a straight waveguide, the present hybrid (de)multiplexer has excess losses (around 1555 nm) of about 0.7 dB, 0.14 dB, 0.25 dB, 0.7 dB, 0.2 dB, 2 dB, 1.5 dB and 2 dB for the TM, TM_1, TM_2, TM_3, TE, TE_1, TE_2 and TE_3 mode channels respectively. The excess loss is mainly caused by the scattering loss due to the sidewall roughness and incomplete coupling in the ADCs due to the fabrication errors.

From Figs. 34(a)–(h), it can also be seen that the crosstalk of eight channels is not so wavelength-sensitive. The crosstalks (around 1555 nm) for the TM_0, TM_1, TM_2 and TM_3 mode channels are about -19 dB, -20 dB, -20 dB and -17.5 dB respectively. In contrast, the four channels for the TE_0, TE_1, TE_2 and TE_3 modes have relatively large crosstalks (i.e., -16 dB, -12 dB, -14 dB and -11 dB, respectively). Since the present hybrid (de)multiplexer works well (with low crosstalk and low loss) over a broad wavelength band, it can be possibly used together with WDM filters to realize a multi-

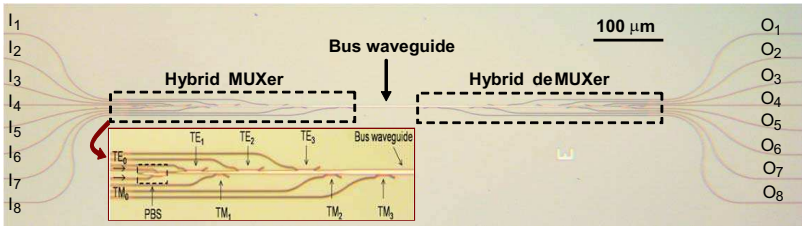

Figure 33. The optical image of the fabricated PIC including the hybrid multiplexer, the multimode bus waveguide and the hybrid demultiplexer. Inset: the optical image of the 8-channels hybrid multiplexer.

dimensional hybrid multiplexing technology to further improve the link capacity.

3.3. Mode-devices for Data Switching/routing in Photonic Networks-on-chip

It is well known that an optical add-drop multiplexer (OADM) is a device used for multiplexing and routing different channels of light into or out of the bus waveguide/fiber, and has been generally used for the construction of optical telecommunication networks. "Add" and "drop" here refer to the capability to add one or more channels to an existing multi-channel signal, and to drop (remove) one or more channels, respectively. For mode-multiplexed optical interconnects, a mode add-drop multiplexer is demanded [76, 77]. Fig. 35(a) shows the schematic configuration of a mode add-drop multiplexer for one channel, which is based on an ADC. As shown in Fig. 35(a), the

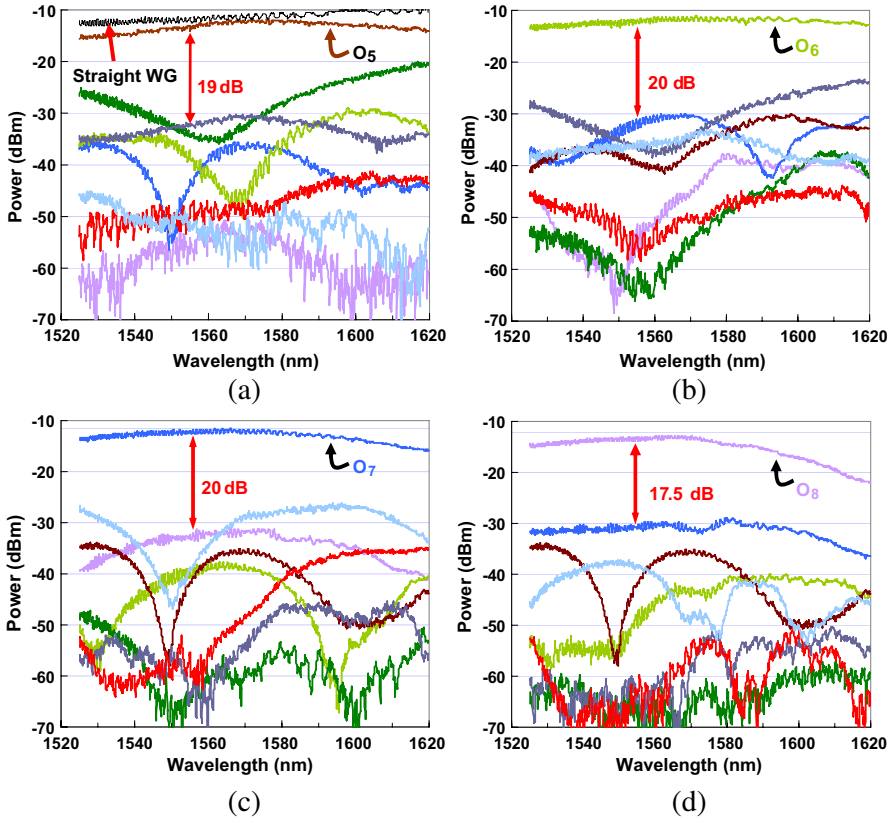

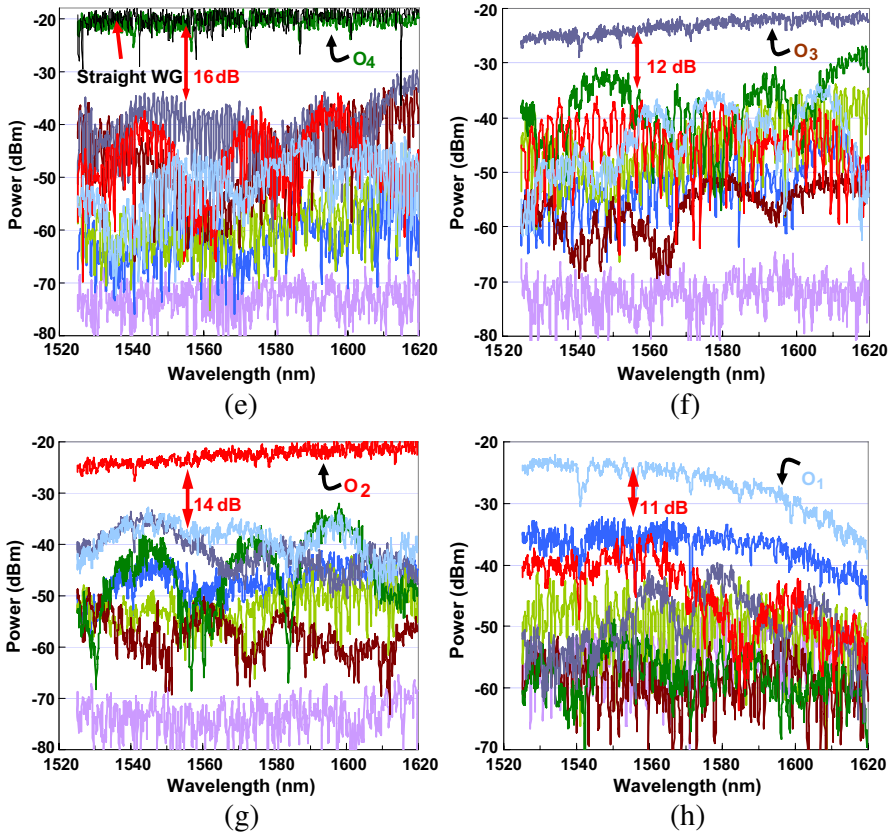

Figure 34. The responses of the eight output ports with the input at port (a) I_5, (b) I_6, (c) I_7, (d) I_8, (e) I_4, (f) I_3, (g) I_2 and (h) I_1 respectively. The transmission responses of straight waveguides for the TM and TE modes (black line) are also shown in (a) and (e).

add port and the drop port are of singlemode waveguide whose width w_{ai} is designed according to the phase matching condition. The data launched at the add port will be added to the i-th mode-channel in the bus waveguide while the original data of the i-th mode channel in the bus waveguide will be dropped in the same time. Such a mode add-drop multiplexer can be cascaded to achieve add-drop multiplexing with multiple channels, as shown in Fig. 35(b).

In order to make the network flexible, the exchange of the data carried by different channels is usually desired. For mode-multiplexed optical interconnects, the key component is the mode-converter, which is in analog to the wavelength converter in WDM systems. Fig. 36(a) shows the proposed mode converter for data exchange between two

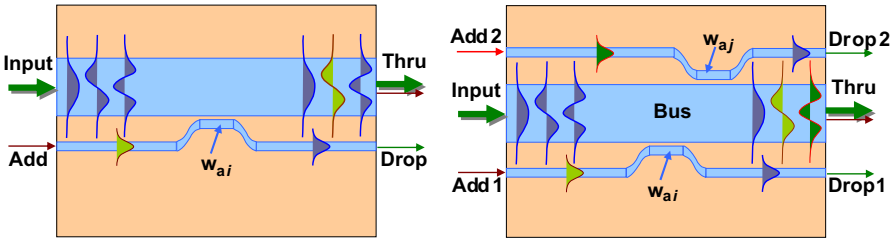

Figure 35. The schematic configuration of a mode add-drop multiplexer (a) with one mode-channel and (b) with more than one mode-channel.

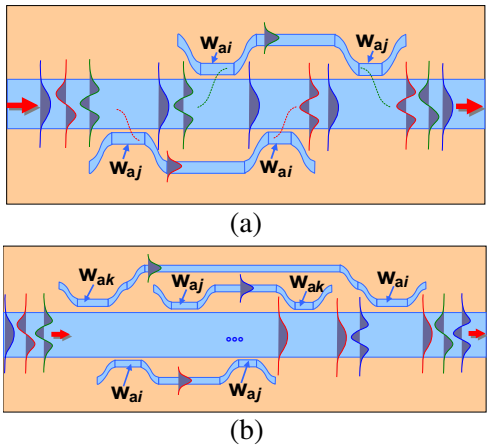

Figure 36. The schematic configuration of a mode converter for data exchange (a) with two mode-channels, and (b) with three mode-channels.

mode-channels. The j-th mode-channel is dropped first with an ADC-based mode add-drop multiplexer working for the j-th channel. The drop data is then converted to the i-th mode on the narrow optical waveguide and finally added to the i-th mode-channel in the bus waveguide by using an ADC-based mode add-drop multiplexer working for the i-th mode-channel. This can be realized easily by choosing different widths (w_{ai}, w_{aj}) for the narrow optical waveguide according to the phase matching condition. This mode converter for data exchange can be expanded to work for more channels, as shown in Fig. 36(b).

When a reconfigurable data-exchange is desired, an $N \times N$ optical switch is needed, as shown in Fig. 37(a). The present reconfigurable

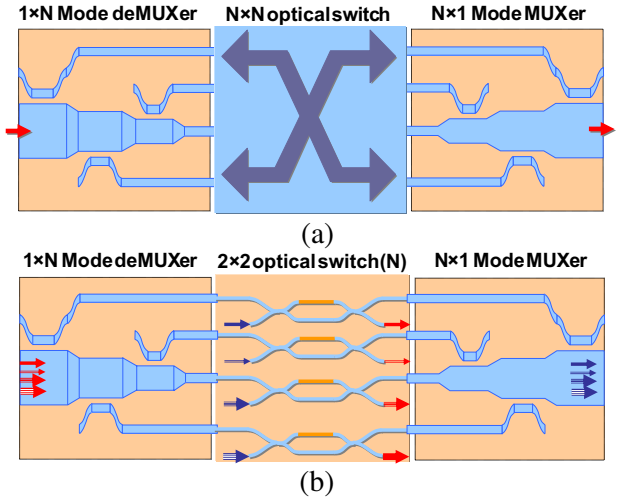

Figure 37. (a) Reconfigurable data exchange module for N mode-channels simultaneously; (b) reconfigurable add-drop mode multiplexer with N mode-channels.

data exchange module consists of a $1 \times N$ mode-demultiplexer, an $N \times N$ optical switch, and an $N \times 1$ mode-multiplexer. In this way, the data exchange is easy and convenient. When the $N \times N$ optical switch is replaced by an array with N elements of 2×2 optical-switch, a reconfigurable add-drop mode multiplexer can be realized (as shown in Fig. 37(b)), which is very similar to that used in a WDM system.

4. CONCLUSION

In this paper, we have given a review on silicon multimode photonic integrated devices for on-chip mulitmode SDM optical interconnects with figures mainly from our own previous work (easier to fix the copyright issue). The configuration for a mulitmode SDM optical interconnect link has been discussed in order to ensure that some regular key devices (including optical modulators and photodetectors) can be used in the transmitters as well as the receivers. Light propagation in two kinds of basic elements (including tapers as well as bending sections) has also been analyzed and discussed. It has been shown that the mode conversion in an adiabatic taper can be very efficient and beneficial to realize the data-exchange between two mode-channels in the bus waveguide. It is also possible to diminish the mode conversion to reduce the mode-channel crosstalk by choosing the taper parameters appropriately. For the multimode bends, some

inter-mode coupling/conversion occurs at the bent-straight junction, which introduces some crosstalk between mode channels. One method of solving this problem is to gradually vary the curvature radius of the bending section and make it adiabatic. The mode converter-multiplexer based on ADCs has been also discussed and reviewed. The ADCs are designed according to the phase matching condition to excite any desired higher-order mode from the fundamental mode of the access waveguide. A four-channel mode converter-(de)multiplexer has been proposed and demonstrated experimentally. In order to improve the link capacity further, a hybrid multiplexer has been proposed to realize the combination of mode-multiplexing and PDM technologies. In particular, we have analyzed in detail in the present paper the fabrication tolerance of our hybrid demultiplexer. Finally we have discussed the demands for devices and several types of optical modules, including add-drop mode multiplexers, mode converters for data exchange with two or more mode-channels, and reconfigurable data exchange module for N mode-channels. These novel devices for mode handling are still under the development.

ACKNOWLEDGMENT

This project was partially supported by a 863 project (No. 2011AA0103 01), the NSFC (11374263), Zhejiang provincial grant (Z201121938) of China, the Science and Technology Department of Zhejiang Province (2010R50007), and the Doctoral Fund of Ministry of Education of China (No. 20120101110094).

REFERENCES

1. Shacham A, K. Bergman, and L. P. Carloni, "Photonic networks-on-chip for future generations of chip multiprocessors," *IEEE Trans. on Computers*, Vol. 57, No. 9, 1246–1260, 2008.
2. Paniccia, M. J., "A perfect marriage: Optics and silicon," *Optik & Photonik*, Vol. 2, 34–38, 2011.
3. Ahn, J., M. Fiorentino, R. G. Beausoleil, et al., "Devices and architectures for photonic chip-scale integration," *Appl. Phys. A*, Vol. 95, 989–997, 2009.
4. Alduino, A., L. Liao, M. R. Jones, et al., "Demonstration of a high speed 4-channel integrated silicon photonics WDM link with hybrid silicon lasers," *Integrated Photonics Research, Silicon and Nanophotonics and Photonics in Switching, OSA Technical Digest (CD)*, paper PDIWI5, Optical Society of America, 2010.

5. Dai, D., L. Liu, S. Gao, D. Xu, and S. He, "Polarization management for silicon photonic integrated circuits," *Laser Photon. Rev.*, Vol. 7, No. 3, 303–328, 2013.
6. Doerr, C. and T. Taunay, "Silicon photonics core-, wavelength-, and polarization-diversity receiver," *IEEE Photon. Tech. Lett.*, Vol. 23, 597–599, 2011.
7. Berdagué, S. and P. Facq, "Mode division multiplexing in optical fibers," *Appl. Opt.*, Vol. 21, 1950–1955, 1982.
8. Randel, S., R. Ryf, A. Sierra, et al., "6 × 56-Gb/s mode-division multiplexed transmission over 33-km few-mode fiber enabled by 6×6 MIMO equalization," *Opt. Express*, Vol. 19, 16697–16707, 2011.
9. Liang, D., M. Fiorentino, T. Okumura, et al., "Electrically-pumped compact hybrid silicon microring lasers for optical interconnects," *Opt. Express*, Vol. 17, 20355–20364, 2009.
10. Saffman, M. and D. Z. Anderson, "Mode multiplexing and holographic demultiplexing communication channels on a multimode fiber," *Opt. Lett.*, Vol. 16, 300–302, 1991.
11. Doerr, C., "Proposed architecture for MIMO optical demultiplexing using photonic integration," *IEEE Photon. Tech. Lett.*, Vol. 23, 1573–1575, 2011.
12. Uematsu, T., Y. Ishizaka, Y. Kawaguchi, K. Saitoh, and M. Koshiba, "Design of a compact two-mode multi/demultiplexer consisting of multi-mode interference waveguides and a wavelength insensitive phase shifter for mode-division multiplexing transmission," *J. Lightwave Technol.*, Vol. 30, No. 15, 2421–2426, 2012.
13. Kawaguchi, Y. and K. Tsutsumi, "Mode multiplexing and demultiplexing devices using multimode Interference couplers," *Electron. Lett.*, Vol. 38, No. 25, 1701–1702, 2002.
14. Dai, D., "Silicon mode-(de)multiplexer for a hybrid multiplexing system to achieve ultrahigh capacity photonic networks-on-chip with a single-wavelength-carrier light," *Asia Communications and Photonics Conference, OSA Technical Digest (Online)*, Paper ATh3B.3, Optical Society of America, 2012.
15. Yadin, Y. and M. Orenstein, "Parallel optical interconnects over multimode waveguides," *J. Lightwave Technol.*, Vol. 24, No. 1, 380–386, 2006.
16. Ryf, R., M. Mestre, A. Gnauck, S. Randel, C. Schmidt, R. Essiambre, P. Winzer, R. Delbue, P. Pupalaikis, A. Sureka, Y. Sun, X. Jiang, D. Peckham, A. McCurdy, and R. Lingle, "Low-loss mode coupler for mode-multiplexed transmission in few-mode

fiber," *National Fiber Optic Engineers Conference, OSA Technical Digest*, Paper PDP5B.5, Optical Society of America, 2012.

17. Chen, H. S., V. Sleiffer, F. Huijskens, R. van Uden, C. Okonkwo, P. Leoni, M. Kuschnerov, L. Gruner-Nielsen, Y. Sun, H. de Waardt, and T. Koonen, "Employing prism-based three-spot mode couplers for high capacity MDM/WDM transmission," *IEEE Photon. Tech. Lett.*, Vol. 25, No. 24, 2474–2477, Dec. 15, 2013.
18. Ryf, R., S. Randel, A. H. Gnauck, C. Bolle, R.-J. Essiambre, P. J. Winzer, D. W. Peckham, A. McCurdy, and R. Lingle, "Space-division multiplexing over 10 km of three-mode fiber using coherent 6×6 MIMO processing," *Optical Fiber Communication Conference and Exposition (OFC/NFOEC), 2011 and the National Fiber Optic Engineers Conference*, 1–3, Mar. 6–10, 2011.
19. Salsi, M., C. Koebele, D. Sperti, P. Tran, P. Brindel, H. Mardoyan, S. Bigo, A. Boutin, F. Verluise, P. Sillard, M. Bigot-Astruc, L. Provost, F. Cerou, and G. Charlet, "Transmission at 2×100 Gb/s, over two modes of 40 km-long prototype few-mode fiber, using LCOS based mode multiplexer and demultiplexer," *Optical Fiber Communication Conference/National Fiber Optic Engineers Conference 2011, OSA Technical Digest (CD)*, Paper PDPB9, Optical Society of America, 2011.
20. Youngquist, R., J. Brooks, and H. Shaw, "Two-mode fiber modal coupler," *Opt. Lett.*, Vol. 9, 177–179, 1984.
21. Youngquist, R., J. Brooks, N. Hanzawa, K. Saitoh, T. Sakamoto, T. Matsui, S. Tomita, and M. Koshiba, "Demonstration of mode-division multiplexing transmission over 10 km two-mode fiber with mode coupler," *Optical Fiber Communication Conference and Exposition (OFC/NFOEC), 2011 and the National Fiber Optic Engineers Conference*, 1–3, Mar. 6–10, 2011.
22. Li, A., A. Al Amin, X. Chen, and W. Shieh, "Transmission of 107-Gb/s mode and polarization multiplexed CO-OFDM signal over a two-mode fiber," *Opt. Express*, Vol. 19, 8808–8814, 2011.
23. Chen, H. S., V. Sleiffer, B. Snyder, M. Kuschnerov, R. van Uden, Y. M. Jung, C. M. Okonkwo, O. Raz, P. O'Brien, H. de Waardt, and T. Koonen, "Demonstration of a photonic integrated mode coupler with MDM and WDM transmission," *IEEE Photon. Tech. Lett.*, Vol. 25, No. 21, 2039–2042, Nov. 1, 2013.
24. Hanzawa, N., K. Saitoh, T. Sakamoto, T. Matsui, K. Tsujikawa, M. Koshiba, and F. Yamamoto, "Two-mode PLC-based mode multi/demultiplexer for mode and wavelength division multiplexed transmission," *Opt. Express*, Vol. 21, 25752–25760, 2013.

25. Gabrielli, L. H., D. Liu, S. G. Johnson, and M. Lipson, "On-chip transformation optics for multimode waveguide bends," *Nature Commun.*, Vol. 3, 1217, 2012.
26. Hanzawa, N., K. Saitoh, T. Sakamoto, T. Matsui, S. Tomita, and M. Koshiba, "Demonstration of mode-division multiplexing transmission over 10 km two-mode fiber with mode coupler," *Optical Fiber Communication Conference/National Fiber Optic Engineers Conference 2011, OSA Technical Digest (CD)*, Paper OWA4, Optical Society of America, 2011.
27. Dai, D., J. Wang, and Y. Shi, "Silicon mode (de)multiplexer enabling high capacity photonic networks-on-chip with a single-wavelength-carrier light," *Opt. Lett.*, Vol. 38, 1422–1424, 2013.
28. Qiu, H. Y., H. Yu, T. Hu, G. M. Jiang, H. F. Shao, P. Yu, J. Y. Yang, and X. Q. Jiang, "Silicon mode multi/demultiplexer based on multimode grating-assisted couplers," *Opt. Express*, Vol. 21, 17904–17911, 2013.
29. Luo, L., N. Ophir, C. Chen, L. H. Gabrielli, C. B. Poitras, K. Bergman, and M. Lipson, "Simultaneous mode and wavelength division multiplexing on-chip," arXiv: 1306.2378, 2013.
30. Dai, D., Y. Shi, and S. He, "Comparative study of the integration density for passive linear planar lightwave circuits based on three different kinds of nanophotonic waveguides," *Appl. Opt.*, Vol. 46, No. 7, 1126–1131, 2007.
31. Bogaerts, W. and S. K. Selvaraja, "Compact single-mode silicon hybrid rib/strip waveguide with adiabatic bends," *IEEE Photon. J.*, Vol. 3, 422–432, 2011.
32. Shani, Y., C. Henry, R. Kistler, K. Orlowsky, and D. Ackerman, "Efficient coupling of a semiconductor laser to an optical fiber by means of a tapered waveguide on silicon," *Appl. Phys. Lett.*, Vol. 55, 2389–2391, 1989.
33. Smith, R., C. Sullivan, G. Vawter, G. Hadley, J. Wendt, M. Snipes, and J. Klem, "Reduced coupling loss using a tapered-rib adiabatic-following fiber coupler," *IEEE Photon. Technol. Lett.*, Vol. 5, 1053–1056, 1993.
34. Zengerle, R., H. Bruckner, H. Olzhausen, and A. Kohl, "Low-loss fiber-chip coupling by buried laterally tapered InP/InGaAsP waveguide structure," *Electron. Lett.*, Vol. 28, 631–632, 1992.
35. Kasaya, K., O. Mitomi, M. Naganuma, Y. Kondo, and Y. Noguchi, "A simple laterally tapered waveguide for low-loss coupling to single-mode fibers," *IEEE Photon. Technol. Lett.*, Vol. 5, 345–347, 1993.

36. Schwander, T., S. Fischer, A. Kramer, M. Laich, K. Luksic, G. Spatschek, and M. Warth, "Simple and low-loss fiber-to-chip coupling by integrated field-matching waveguide in InP," *Electron. Lett.*, Vol. 29, 326–328, 1993.
37. Yang, L., D. Dai, B. Yang, Z. Sheng, and S. He, "Characteristic analysis of tapered lens fibers for light focusing and butt-coupling to a Si rib waveguide," *Appl. Opt.*, Vol. 48, 672–678, 2009.
38. Dai, D., S. He, and H. K. Tsang, "Bilevel mode converter between a silicon nanowire waveguide and a larger waveguide," *J. Lightwave Technol.*, Vol. 24, 2428–2433, 2006.
39. Barkai, A., A. Liu, D. Kim, R. Cohen, N. Elek, H.-H. Chang, B. H. Malik, R. Gabay, R. Jones, M. Paniccia, and N. Izhaky, "Double-stage taper for coupling between SOI waveguides and single-mode fiber," *J. Lightwave Technol.*, Vol. 26, 3860–3865, 2008.
40. Shani, Y., C. H. Henry, R. C. Kistler, R. F. Kazarinov, and K. J. Orlowsky, "Integrated optic adiabatic devices on silicon," *IEEE J. Quant. Electron.*, Vol. 27, 556–566, 1991.
41. Fan, R. S. and R. B. Hooker, "Tapered polymer single-mode waveguides for mode transformation," *J. Lightwave Technol.*, Vol. 17, 466–474, 1999.
42. Wörhoff, K., P. V. Lambeck, and A. Driessen, "Design, tolerance analysis, and fabrication of silicon oxynitride based planar optical waveguides for communication devices," *J. Lightwave Technol.*, Vol. 17, 1401–1407, 1999.
43. Sewell, P., T. M. Benson, and P. C. Kendall, "Rib waveguide spot-size transformers: Modal properties," *J. Lightwave Technol.*, Vol. 17, 848–856, 1999.
44. Sasaki, K., F. Ohno, A. Motegi, and T. Baba, "Arrayed waveguide grating of $70 \times 60\ \mu m^2$ size based on Si photonic wire waveguides," *Electron. Lett.*, Vol. 41, 801–802, 2005.
45. Dai, D., L. Liu, L. Wosinski, and S. He, "Design and fabrication of ultra-small overlapped AWG demultiplexer based on alpha-Si nanowire waveguides," *Electron. Lett.*, Vol. 42, 400–402, 2006.
46. Bogaerts, W., S. K. Selvaraja, P. Dumon, J. Brouckaert, K. de Vos, D. van Thourhout, and R. Baets, "Silicon-on-insulator spectral filters fabricated with CMOS technology," *IEEE J. Sel. Top. Quant. Electron.*, Vol. 16, 33–44, 2010.
47. Fukuda, H., K. Yamada, T. Tsuchizawa, T. Watanabe, H. Shinojima, and S. Itabashi, "Silicon photonic circuit with polarization diversity," *Opt. Express*, Vol. 16, 4872–4880, 2008.

48. Bogaerts, W., P. Dumon, D. V. Thourhout, D. Taillaert, P. Jaenen, J. Wouters, S. Beckx, V. Wiaux, and R. G. Baets, "Compact wavelength-selective functions in silicon-on-insulator photonic wires," *IEEE J. Sel. Top. Quant. Electron.*, Vol. 12, 1394–1401, 2006.
49. Soltani, M., S. Yegnanarayanan, and A. Adibi, "Ultra-high Q planar silicon microdisk resonators for chip-scale silicon photonics," *Opt. Express*, Vol. 15, 4694–4704, 2007.
50. Boyraz, O. and B. Jalali, "Demonstration of a silicon Raman laser," *Opt. Express*, Vol. 12, 5269–5273, 2004.
51. Li, C., L. Zhou, and A. W. Poon, "Silicon microring carrier-injection-based modulators/switches with tunable extinction ratios and OR-logic switching by using waveguide cross-coupling," *Opt. Express*, Vol. 15, 5069–5076, 2007.
52. Rong, H., R. Jones, A. Liu, O. Cohen, D. Hak, A. Fang, and M. Paniccia, "A continuous-wave Raman silicon laser," *Nature*, Vol. 433, 725–728, 2005.
53. Xu, Q., B. Schmidt, S. Pradhan, and M. Lipson, "Micrometre-scale silicon electro-optic modulator," *Nature*, Vol. 435, 325–327, 2005.
54. Barrios, C. A., V. R. Almeida, R. Panepucci, and M. Lipson, "Electrooptic modulation of silicon-on-insulator submicrometer-size waveguide devices," *J. Lightwave Technol.*, Vol. 21, 2332–2339, 2003.
55. Tang, Y., H.-W. Chen, S. Jain, J. D. Peters, U. Westergren, and J. E. Bowers, "50 Gb/s hybrid silicon traveling-wave electroabsorption modulator," *Opt. Express*, Vol. 19, 5811–5816, 2011.
56. Mertens, K., B. Scholl, and H. Schmitt, "New highly efficient polarization converters based on hybrid supermodes," *J. Lightwave Technol.*, Vol. 13, 2087–2092, 1995.
57. Liu, L., Y. Ding, K. Yvind, and J. M. Hvam, "Silicon-on-insulator polarization splitting and rotating device for polarization diversity circuits," *Opt. Express*, Vol. 19, 12646–12651, 2011.
58. Dai, D., Z. Wang, N. Julian, and J. E. Bowers, "Compact broadband polarizer based on shallowly-etched silicon-on-insulator ridge optical waveguides," *Opt. Express*, Vol. 18, 27404–27415, 2010.
59. Tummidi, R. S., T. G. Nguyen, A. Mitchell, and T. L. Koch, "An ultra-compact waveguide polarizer based on 'anti-magic widths'," *2011 8th IEEE International Conference on Group IV Photonics (GFP)*, 104–106, London, UK, Sep. 14–16, 2011.
60. Vermeulen, D., S. Selvaraja, W. A. D. De Cort, N. A. Yebo,

E. Hallynck, K. De Vos, P. P. P. Debackere, P. Dumon, W. Bogaerts, G. Roelkens, D. Van Thourhout, and R. Baets, "Efficient tapering to the fundamental quasi-TM mode in asymmetrical waveguides," *European Conference on Integrated Optics*, 2010.

61. Dai, D. and J. E. Bowers, "Novel concept for ultracompact polarization splitter-rotator based on silicon nanowires," *Opt. Express*, Vol. 19, 10940–10949, 2011.
62. Dai, D., J. He, and S. He, "Elimination of multimode effects in a silicon-on-insulator etched diffraction grating demultiplexer with bi-level taper structure," *IEEE J. Sel. Top. Quant. Electron.*, Vol. 11, 439–443, 2005.
63. Schmid, J. H., B. Lamontagne, P. Cheben, A. Delâge, S. Janz, A. Densmore, J. Lapointe, E. Post, P. Waldron, and D.-X. Xu, "Mode converters for coupling to high aspect ratio silicon-on-insulator channel waveguides," *IEEE Photon. Technol. Lett.*, Vol. 19, 855–857, 2007.
64. Dai, D., Y. Tang, and J. E. Bowers, "Mode conversion in tapered submicron silicon ridge optical waveguides," *Opt. Express*, Vol. 20, No. 12, 13425–13439, 2012.
65. Sorin, W., B. Kim, and H. Shaw, "Highly selective evanescent modal filter for two-mode optical fibers," *Opt. Lett.*, Vol. 11, 581–583, 1986.
66. Li, A., X. Chen, A. A. Amin, and W. Shieh, "Fused fiber mode couplers for few-mode transmission," *IEEE Photon. Tech. Lett.*, Vol. 24, No. 21, 1953–1956, Nov. 1, 2012.
67. Love, J. and N. Riesen, "Mode-selective couplers for few-mode optical fiber networks," *Opt. Lett.*, Vol. 37, 3990–3992, 2012.
68. Saitoh, F., K. Saitoh, and M. Koshiba, "A design method of a fiber-based mode multi/demultiplexer for mode-division multiplexing," *Opt. Express*, Vol. 18, 4709–4716, 2010.
69. Leon-Saval, S., A. Argyros, and J. Bland-Hawthorn, "Photonic lanterns: A study of light propagation in multimode to single-mode converters," *Opt. Express*, Vol. 18, 8430–8439, 2010.
70. Fontaine, N. K., C. R. Doerr, M. A. Mestre, R. R. Ryf, P. J. Winzer, L. L. Buhl, Y. Sun, X. L. Jiang, and R. Lingle, "Space-division multiplexing and all-optical MIMO demultiplexing using a photonic integrated circuit," *Optical Fiber Communication Conference and Exposition (OFC/NFOEC)*, 1–3, 2012.
71. Wohlfeil, B., C. Stamatiadis, L. Zimmermann, and K. Petermann, "Compact fiber grating coupler on SOI for coupling of higher order

fiber modes," *Optical Fiber Communication Conference/National Fiber Optic Engineers Conference 2013, OSA Technical Digest (Online)*, Paper OTh1B.2, Optical Society of America, 2013.

72. Ding, Y., H. Ou, J. Xu, and C. Peucheret, "Silicon photonic integrated circuit mode multiplexer," *IEEE Photon. Tech. Lett.*, Vol. 25, No. 7, 648–651, 2013.
73. Koonen, A. M. J., H. S. Chen, H. P. A. van den Boom, and O. Raz, "Silicon photonic integrated mode multiplexer and demultiplexer," *IEEE Photon. Tech. Lett.*, Vol. 24, No. 21, 1961–1964, 2012.
74. Huang, Y., G. Xu, and S. T. Ho, "An ultracompact optical mode order converter," *IEEE Photon. Tech. Lett.*, Vol. 18, No. 21, 2281–2283, 2006.
75. Uematsu, T., Y. Ishizaka, Y. Kawaguchi, K. Saitoh, and M. Koshiba, "Design of a compact two-mode multi/demultiplexer consisting of multi-mode interference waveguides and a wavelength insensitive phase shifter for mode-division multiplexing transmission," *J. Lightwave Technol.*, Vol. 30, No. 15, 2421–2426, 2012.
76. Greenberg, M. and M. Orenstein, "Multimode add-drop multiplexing by adiabatic linearly tapered coupling," *Opt. Express*, Vol. 13, 9381–9387, 2005.
77. Greenberg, M. and M. Orenstein, "Mode add drop for optical interconnects based on adiabatic high order mode couplers," *Quantum Electronics and Laser Science Conference (QELS'05)*, Vol. 2, 942–944, 2005.
78. Xing, J. J., Z. Y. Li, X. Xiao, J. Z. Yu, and Y. D. Yu, "Two-mode multiplexer and demultiplexer based on adiabatic couplers," *Opt. Lett.*, Vol. 38, 3468–3470, 2013.
79. Love, J. D., R. W. C. Vance, and A. Joblin, "Asymmetric, adiabatic multipronged planar splitters," *Optical and Quantum Electronics*, Vol. 28, 353–369, 1996.
80. Lee, B.-T. and S.-Y. Shin, "Mode-order converter in a multimode waveguide," *Opt. Lett.*, Vol. 28, 1660–1662, 2003.
81. Andy, L. Y. L., Y. S. Yong, A. H. You, S. F. Chien, and C. F. Teo, "A five-order mode converter for multimode waveguide," *IEEE Photon. Techn. Lett.*, Vol. 16, No. 7, 1673–1675, 2004.
82. Riesen, N. and J. D. Love, "Spatial mode-division-multiplexing of few-mode fiber," *European Conference and Exhibition on Optical Communication, OSA Technical Digest (Online)*, Paper P2.14, Optical Society of America, 2012.
83. Riesen, N. and J. D. Love, "Design of mode-sorting asymmetric Y-junctions," *Appl. Opt.*, Vol. 51, 2778–2783, 2012.

84. Driscoll, J., R. Grote, B. Souhan, J. Dadap, M. Lu, and R. Osgood, "Asymmetric Y junctions in silicon waveguides for on-chip mode-division multiplexing," *Opt. Lett.*, Vol. 38, 1854–1856, 2013.
85. Chen, W. W., P. J. Wang, and J. Y. Yang, "Mode multi/demultiplexer based on cascaded asymmetric Y-junctions," *Opt. Express*, Vol. 21, 25113–25119, 2013.
86. Bagheri, S. and W. M. J. Green, "Silicon-on-insulator mode-selective add-drop unit for on-chip mode-division multiplexing," *The 6th IEEE International Conference on Group IV Photonics (GFP'09)*, 166–168, 2009.
87. Dai, D., "Silicon polarization beam splitter based on an asymmetrical evanescent coupling system with three optical waveguides," *J. Lightwave Technol.*, Vol. 30, No. 20, 3281–3287, 2012.
88. Augustin, L. M., J. J. G. M. van der Tol, R. Hanfoug, W. J. M. de Laat, M. J. E. van de Moosdijk, P. W. L. van Dijk, Y.-S. Oei, and M. K. Smit, "A single etch-step fabrication-tolerant polarization splitter," *J. Lightwave Technol.*, Vol. 25, No. 3, 740–746, 2007.
89. Greenberg, M. and M. Orenstein, "Multimode add-drop multiplexing by adiabatic linearly tapered coupling," *Opt. Express*, Vol. 13, 9381–9387, 2005.
90. Ding, Y., J. Xu, F. Da Ros, B. Huang, H. Ou, and C. Peucheret, "On-chip two-mode division multiplexing using tapered directional coupler-based mode multiplexer and demultiplexer," *Opt. Express*, Vol. 21, 10376–10382, 2013.
91. Taillaert, D., W. Bogaerts, P. Bienstman, T. Krauss, P. van Daele, I. Moerman, S. Verstuyft, K. de Mesel, and R. Baets, "An out-of-plane grating coupler for efficient butt-coupling between compact planar waveguides and single-mode fibers," *IEEE J. Quantum Electron.*, Vol. 38, No. 7, 949–955, 2002.
92. McNab, S., N. Moll, and Y. Vlasov, "Ultra-low loss photonic integrated circuit with membrane-type photonic crystal waveguides," *Opt. Express*, Vol. 11, 2927–2939, 2003.
93. Wang, J., S. He, and D. Dai, "On-chip silicon 8-channel hybrid (de)multiplexer enabling simultaneous mode- and polarization-division-multiplexing," *Laser & Photonics Reviews (submitted). Part of its results was also presented briefly in Asia Communications and Photonics Conference*, OSA Technical Digest (Online), Optical Society of America, 2013.